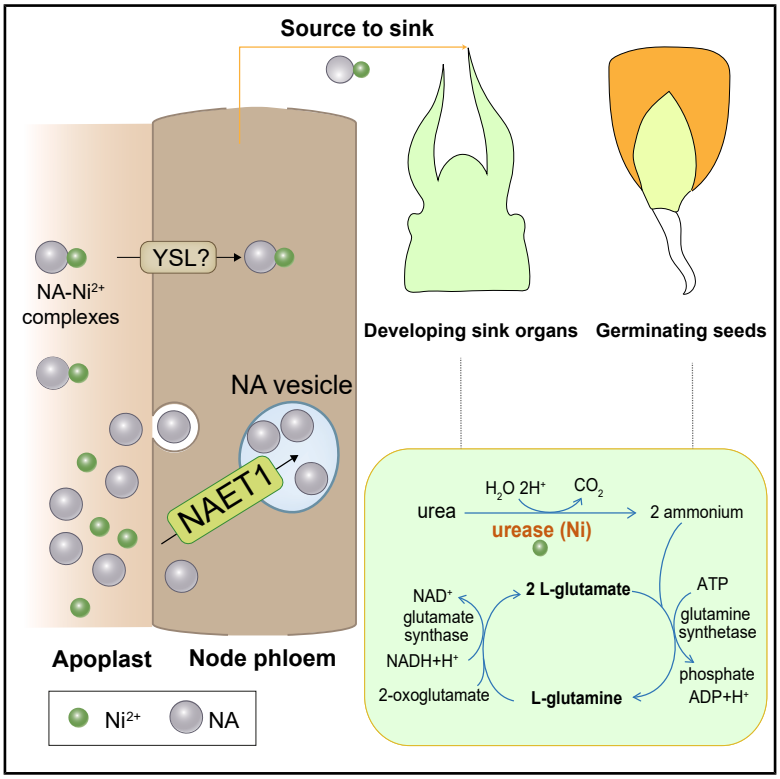
Cell

Nicotianamine-driven nickel transport to sink organs underpins maize productivity

Graphical abstract



Highlights

- Genetic evidence establishes the essentiality of Ni in maize
- ZmNAET1 mediates NA secretion to facilitate Ni translocation to sink organs
- Urease is active in maize sink organs and requires Ni for urea N reutilization
- Ni contributes to seed germination and productivity in maize

Authors

Zhen-Fei Chao, Yuanyuan Chen, Jia-Chen Wu, ..., Nicolaus von Wirén, Jianbing Yan, Dai-Yin Chao

Correspondence

yjianbing@mail.hzau.edu.cn (J.Y.), dychao@cemps.ac.cn (D.-Y.C.)

In brief

A node-phloem-localized nicotianamine efflux transporter in maize regulates Ni delivery to sink organs, including seeds, where Ni-dependent urease activity promotes amino acid metabolism, revealing an unappreciated role of Ni in the yield formation of graminaceous plants.

Chao et al., 2027, Cell *190*, 1–14
February 4, 2027 © 2026 Elsevier Inc. All rights reserved, including those for text and data mining, AI training, and similar technologies.
https://doi.org/10.1016/j.cell.2026.10.035

CellPress

Please cite this article in press as: Chao et al., Nicotianamine-driven nickel transport to sink organs underpins maize productivity, Cell (2027), https://doi.org/10.1016/j.cell.2026.10.035

Cell

CellPress

Article

Nicotianamine-driven nickel transport to sink organs underpins maize productivity

Zhen-Fei Chao,[1,7,9] Yuanyuan Chen,[2,3,9] Jia-Chen Wu,[1,4,9] Ya-Ling Wang,[1] Yingjie Xiao,[3,5] Yong Peng,[3,5] Lu-Yu Fan,[1,4] Xiaqing Wang,[6] Mei-Ling Han,[1] Hai-Jun Liu,[3,5] Nicolaus von Wirén,[7] Jianbing Yan,[3,5,*] and Dai-Yin Chao[1,8,10,*]

[1]National Key Laboratory of Plant Design, CAS Center for Excellence in Molecular Plant Sciences, Chinese Academy of Sciences, Shanghai 200032, China

[2]Guangdong Key Laboratory for Crop Germplasm Resources Preservation and Utilization, Agro-Biological Gene Research Center, Guangdong Academy of Agricultural Sciences, Guangzhou 510640, China

[3]National Key Laboratory of Crop Genetic Improvement, Huazhong Agricultural University, Wuhan 430070, China

[4]University of Chinese Academy of Sciences, Beijing 100049, China

[5]Hubei Hongshan Laboratory, Wuhan 430070, China

[6]Beijing Key Laboratory of Maize DNA Fingerprinting and Molecular Breeding, Maize Research Institute, Beijing Academy of Agriculture & Forestry Sciences (BAAFS), Beijing 100097, China

[7]Molecular Plant Nutrition, Department of Physiology & Cell Biology, Leibniz Institute of Plant Genetics and Crop Plant Research (IPK), Corrensstr. 3, 06466 Gatersleben, Germany

[8]Shanghai Zhangjiang Smart Breeding Center, Shanghai 201210, China

[9]These authors contributed equally

[10]Lead contact

*Correspondence: yjianbing@mail.hzau.edu.cn (J.Y.), dychao@cemps.ac.cn (D.-Y.C.)

https://doi.org/10.1016/j.cell.2026.10.035

SUMMARY

Nickel (Ni), the last essential trace element identified in plants, has long been enigmatic regarding the genetic basis underlying its homeostasis and its agricultural significance. Using genome-wide association analysis, we identified ZmNAET1 as a key transporter controlling Ni allocation to seeds. Mechanistically, ZmNAET1 mediates nicotianamine secretion and enables nicotianamine-dependent phloem loading of Ni in nodes and subsequent Ni translocation into sink organs. Mutants lacking ZmNAET1 exhibit significant yield penalties, decreased seed germination velocity, and drastically shortened seed longevity. In an irreplaceable role, supplemented Ni fully rescued seed germination and proper vegetative development of the mutants. We show that NAET1-dependent delivery of Ni to urease is essential for amino acid turnover in developing sink organs, revealing an unappreciated role of Ni in yield formation of graminaceous plants. This study uncovers an underestimated requirement for nicotianamine and Ni and opens a new research avenue toward optimizing micronutrient provision for cereal crop productivity.

INTRODUCTION

Liebig's law of the minimum, formulated in the 19th century, highlights the significance of essential mineral elements in agriculture.[1] Nickel (Ni) was suggested as a beneficial element for crops as early as the 1940s.[2] However, it was not recognized as an essential element for plants in general until the 1980s,[3–5] when most other essential elements had been identified for over 40 years. Ni was found to be a cofactor of urease,[6,7] confirming its important role in nitrogen metabolism. Eskew et al. (1983) and Brown et al. (1987) grew soybean and barley in an ultra-purified culture solution without Ni for two or three generations and established that Ni is an essential element for plants from the perspective of plant physiology.[3–5] However, unlike other essential elements, the agricultural importance of Ni has not been widely acknowledged. This may be attributed to the perception of low Ni demand in plants, but it also likely stems from the lack of knowledge about the genetic and molecular basis underlying crop Ni homeostasis.

Phytochemical evidence from a study of Ni-hyperaccumulators of the Brassicaceae family has shown that histidine serves as a high-affinity chelator for Ni and suggests its involvement in xylem Ni translocation.[8–10] However, the transporters for histidine or histidine-Ni have not yet been identified, and the phloem-mediated source-to-sink mobility of Ni remains unknown. It is therefore difficult to establish an in-depth understanding of the role and transport mechanism of Ni in plants. Nicotianamine (NA) was first identified as a precursor of DMA (2′-deoxymugineic acid) in graminaceous plants,[11] and it was then found to be a chelator that facilitates root uptake, cellular

All rights are reserved, including those for text and data mining, AI training, and similar technologies.

Please cite this article in press as: Chao et al., Nicotianamine-driven nickel transport to sink organs underpins maize productivity, Cell (2027), https://doi.org/10.1016/j.cell.2026.10.035

compartmentalization, xylem loading, phloem loading, or seed uploading of Cu, Co, Fe, and Ni in dicotyledonous plants.[12–14] However, in graminaceous plants, the function of NA in facilitating metal transport remains largely unclear beyond acting as a precursor of DMA.

Maize (*Zea mays* L.) is one of the world's most important crops,[15] and it relies heavily on urea as a major form of nitrogen fertilizer input.[16] Although urea is generally assumed to be hydrolyzed in soil prior to root uptake, it is also continuously generated internally through arginine catabolism and protein turnover, implying a sustained Ni requirement.[17] Yet, the relevance of Ni and urea in protein turnover and nitrogen metabolism in developing sink organs, where nitrogen demand is high,[18] remains poorly understood.

Here, we employed an association mapping approach to identify the NA efflux transporter *ZmNAET1* as the causal gene responsible for natural variation in Ni accumulation in maize kernels. Our data establish that ZmNAET1-mediated NA secretion facilitates Ni translocation into developing sink organs, including seeds, thereby enhancing maize growth and seed vigor. This study not only uncovers a distinct role of NA and NA efflux transporter (NAET) proteins in regulating transition metal homeostasis in graminaceous and nongraminaceous plants but also demonstrates that Ni-mediated urea hydrolysis is a critical factor in cereal crop productivity.

RESULTS

A major QTL specifically controls kernel Ni concentration in maize

We measured the Ni concentrations in kernels of the complete-diallel plus unbalanced breeding-derived inter-cross (CUBIC) population,[19] comprising 1,404 individuals grown in Hainan Province (Kernel_1, year 2014). The observed kernel Ni concentrations ranged from 0.0075 to 0.4820 μg g^{-1} dry weight (DW) across the population (Figure S1; Table S1). In combination with the high-quality genomic sequence dataset, we conducted a large-scale genome-wide association study (GWAS) and identified a major quantitative trait locus (QTL) controlling kernel Ni concentration on chromosome 9 (Figure 1A). We repeated the experiment in 2016 by cultivating the population in a different field in Hainan (Kernel_2, year 2016) and identified the same locus (Figures 1B and S1B). In the GWAS for the Kernel_2 test (which was used for all subsequent analyses unless otherwise stated), the most significant single-nucleotide polymorphism (SNP) at chr9_2212791 (p value = 2.22×10^{-30}) explained 14.44% of the total phenotypic variance in the kernel Ni concentration.

Surrounding the peak SNP chr9.s_2212791, there were 3,417 SNPs significantly associated with kernel Ni concentration in the CUBIC population. To distinguish discrete QTL intervals from the extensive distribution of significant associations, the significant SNPs were first grouped into 20-kb sliding windows, and windows containing at least two consecutive significant SNPs were retained. Adjacent significant windows were then merged when their linkage disequilibrium (LD) reached $r^2 \geq 0.2$, resulting in a continuous LD-supported interval of approximately 400 kb. This interval represents a major-effect QTL associated with kernel Ni concentration in maize and encompasses seven annotated genes (Table S2). Among these genes, GRMZM2G057611 (Zm00001eb371840 in Zm-B73-REFERENCE-NAM-5.0) was annotated as a nitrate/peptide transporter, and its closest orthologs in *Arabidopsis* are NAETs[20] (Figure S2). Notably, the peak SNP chr9_2212791 resides in the second intron (379 bp to the start codon) of GRMZM2G057611 (Figure 1C), supporting its role as the best candidate for controlling the natural variation of Ni accumulation in maize kernels. Although NAET1 and NAET2 have not yet been shown to affect the long-distance transport of Ni in *Arabidopsis*, they are indeed required for the translocation of iron (Fe), copper (Cu), and cobalt (Co) to seeds.[20] Considering that graminaceous plants and nongraminaceous plants may employ different strategies for the long-distance transport of transition metals,[13,21] we therefore designated GRMZM2G057611 as *ZmNAET1* and prioritized this gene for further validation.

The eight most significant SNPs within the 2-kb promoter and gene body of *ZmNAET1* showed moderate to strong LD with each other (r^2 = 0.24–0.95), indicating that they largely represent correlated association signals at this locus (Figure S3A; Table S3). Based on these most significant SNPs, 1,253 lines out of the CUBIC population were classified into five haplotypes (hapA, hapB, hapC, hapD, and hapE) (Figure 1C; Table S1). Among these five haplotypes, there were no significant differences in Ni concentration and ZmNAET1 expression level (Figures S3B and S3C), indicating that the variations defining these haplotypes are not related to the phenotype. Interestingly, we found that the allelic variations of hapA originated exclusively from the parental line HUANGC, whereas the allelic variations of the other four haplotypes were derived from the other twenty-three parental lines. Therefore, we grouped hapB, hapC, hapD, and hapE as Hap2 and assigned hapA as Hap1 (Figure 1C; Table S1).

The Hap1 allele is present in 15.9% of the CUBIC population, which is almost 4 times higher than its theoretical frequency. Compared with the Hap2 group, which exhibited comparable kernel Ni concentrations (Figure S3B), Hap1 lines accumulated, on median, 60% more Ni in their kernels (Figure 1D). Meanwhile, all other transition metals except Zn showed no difference between the two haplotypes. There was a slight difference in Zn (3.5% in year 2014 and 6.2% in year 2016) between the two haplotypes, but the Hap1 lines were lower than the Hap2 lines, in the opposite direction to that of Ni (Figure S4; Table S1). The eight variants showed significant allelic effects on kernel Ni concentration (Table S4) and were also associated with ZmNAET1 expression levels (Table S5). This suggests that the polymorphisms in the promoter or intron regions likely drive the natural variation in kernel Ni concentration by affecting gene expression. We then sequenced the entire genomic region of the two alleles of *ZmNAET1* in 24 parents and identified a 941-bp insertion in the second intron of the Hap1 allele (Figure 1C). Such a structural variation (SV) might affect the expression of *ZmNAET1*.

The tissue expression profile of *ZmNAET1* in B73 showed that this gene was relatively highly expressed in the shank, which links the ear and the main stalk, as well as in the stem (Figure S3D). An analysis of RNA sequencing (RNA-seq) data

Please cite this article in press as: Chao et al., Nicotianamine-driven nickel transport to sink organs underpins maize productivity, Cell (2027), https://doi.org/10.1016/j.cell.2026.10.035

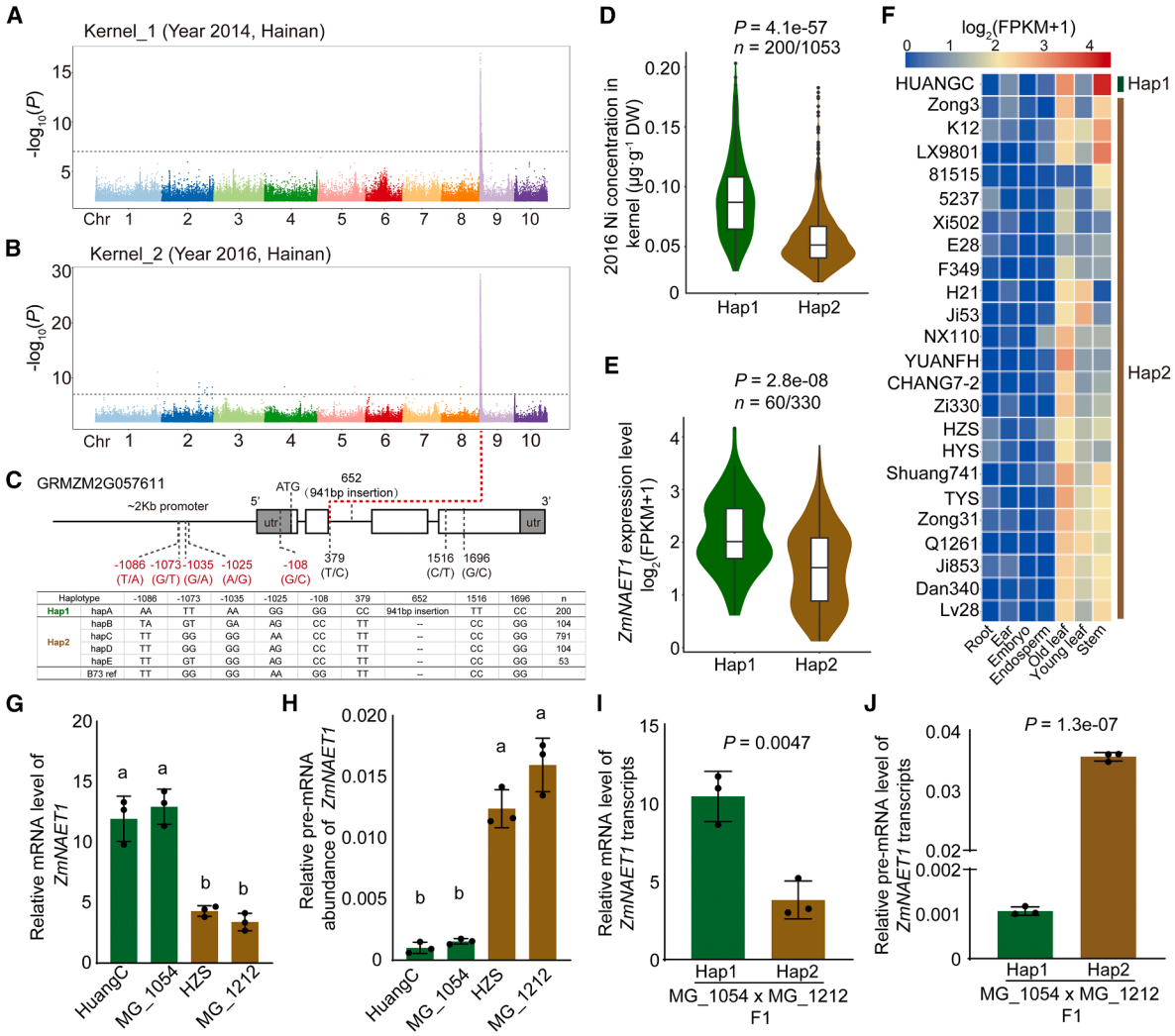


Figure 1. GWAS for the kernel Ni concentrations in CUBIC

(A and B) Manhattan plot of Ni concentrations in Kernel_1 and Kernel_2 obtained by GWAS. Kernel_1 and Kernel_2 represent kernels of the CUBIC population planted in 2014 (A) and 2016 (B) in different plots of Hainan Province. The black dashed line indicates the cut-off $-\log_{10}(p) = 7.0$.

(C) Gene model of GRMZM2G057611 (ID in B73-REFERENCE-NAM-5.0: *Zm00001eb371840*) and two major haplotypes (Hap1 and Hap2) and five sub-haplotypes (hapA to hapE) defined by polymorphisms in this gene and 2-kb promoter.

(D) Ni concentrations in kernels of the two haplotypes among the CUBIC offspring in Kernel_2.

(E) The expression level of *ZmNAET1* in the two haplotypes among CUBIC offspring.

(F) The expression level of *ZmNAET1* in different tissues of the CUBIC parents.

(G) Relative mRNA abundance of *ZmNAET1* in stems of parents and CUBIC progenies. HUANGC (Hap1) and HZS (Hap2) are parent lines, whereas MG_1054 (Hap1) and MG_1212 (Hap2) are CUBIC progenies.

(H) Relative pre-mRNA abundance of *ZmNAET1* in stems of the parents and CUBIC progenies. Expression levels were normalized to that of Zm*STG1* (B73-REFERENCE-NAM-5.0 ID: *Zm00001eb159420*) and calculated using the $2^{-\Delta Ct}$ method. Data are presented as mean ± SDs. $n = 3$ biologically independent samples from three plants.

(I and J) Relative allelic mRNA (I) and pre-mRNA (J) abundance of *ZmNAET1* in nodes of F1 progenies from the cross of MG_1054 and MG_1212, detected using Hap1 specific and Hap2 specific RT-qPCR primer pairs. Data are presented as mean ± SDs. $n = 3$ biologically independent samples from three plants.

Statistical significance was determined by two-sided Student's *t* test (D, E, I, and J). Different letters indicate significant differences in the same group ($p < 0.05$), as determined by one-way ANOVA followed by Tukey's post hoc test (G and H). In violin plots (D and E), the center line indicates the median, and the bounds of the box indicate the interquartile range. The width of each violin represents the density of observations.

from390 CUBIC lines with genotypes defining the haplotypes showed that the Hap1 lines express significantly higher levels of *ZmNAET1* than the Hap2 lines (Figures 1E and S4D–S4F; Table S1). In addition, using other RNA-seq data from 24 parents across different tissues, we found that only HUANGC expresses the highest levels of *ZmNAET1* in the stem compared with the other parents (Figure 1F; Table S6). These data support the hypothesis that *ZmNEAT1* is responsible for the natural variation

Please cite this article in press as: Chao et al., Nicotianamine-driven nickel transport to sink organs underpins maize productivity, Cell (2027), https://doi.org/10.1016/j.cell.2026.10.035

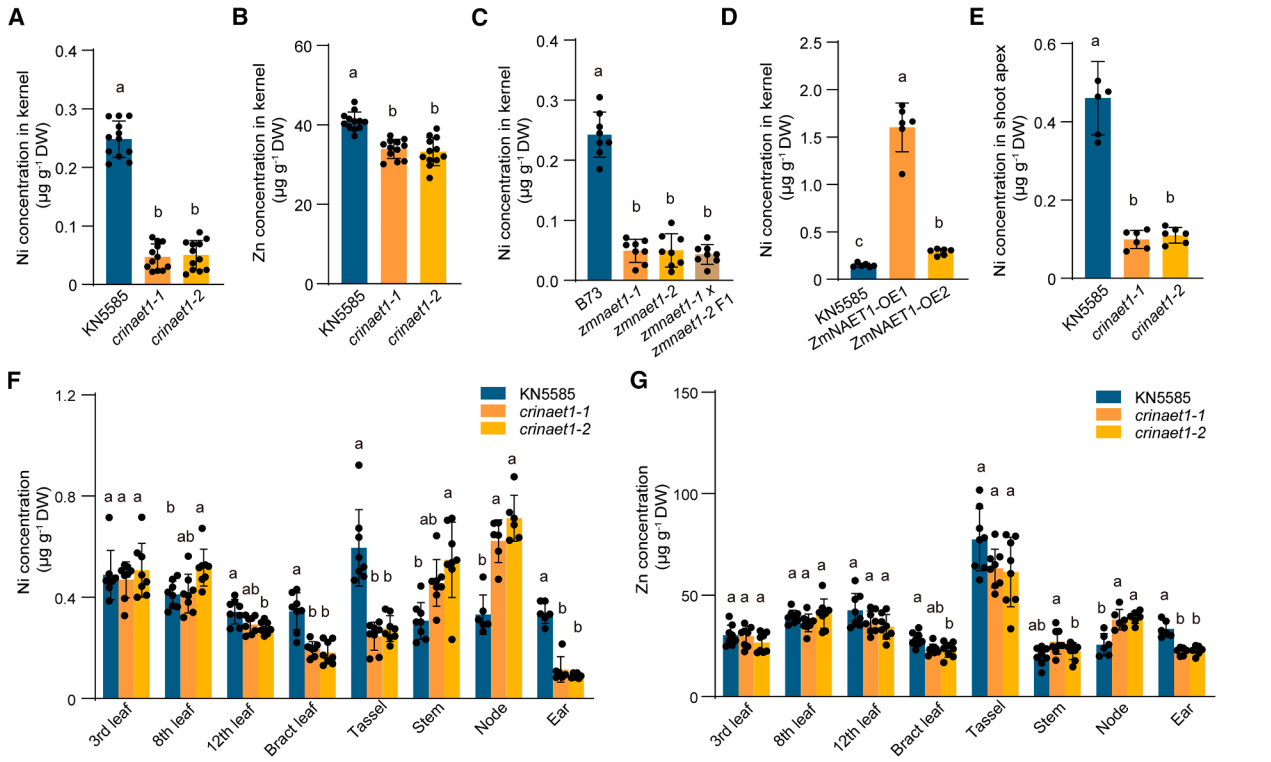


Figure 2. *ZmNAET1* regulates Ni accumulation in maize kernel

(A) Ni concentrations in mature kernels of the *crinaet1* mutants and KN5585. Bars represent means ± SD. $n = 12$.

(B) Zn concentrations in mature kernels of the *crinaet1*mutants and KN5585. Bars represent means ± SD. $n = 12$.

(C) Ni concentrations in mature kernels of the EMS *zmnaet1* mutants and B73. Ni concentrations in mature kernels of F1 progeny derived from crosses between the two EMS mutants are also shown. Bars represent means ± SD. $n = 8$.

(D) Ni concentrations in KN5585 and two *ZmNAET1* overexpression lines. Bars represent means ± SD. $n = 6$. Seeds from 6 plants were analyzed.

(E) Ni concentrations in the shoot apex of *crinaet1* mutants and KN5585. Shoot apex was collected 4 weeks after germination in the field. Bars represent means ± SD. $n = 6$ independent samples from different plants.

(F and G) Ni (F) and Zn (G) concentrations in different organs of *crinaet1* mutants and KN5585. Bars represent means ± SD. $n = 6$.

Different letters indicate significant differences in the same group ($p < 0.05$), as determined by one-way ANOVA followed by Tukey's post hoc test.

in kernel Ni concentration and that Hap1 *ZmNEAT1* represents a hyperfunctional allele.

There are four SNPs in the promoter region and one SNP and one SV in the second intron (Figure 1C). Given the higher expression of the Hap1 *ZmNAET1* allele, these regulatory and intronic polymorphisms may contribute to more efficient transcription or splicing rates. To check these possibilities, we examined the relative mRNA (Figure 1G) and nuclear pre-mRNA abundances (Figure 1H) of *ZmNAET1* in HUANGC (Hap1) and HZS (Hap2), two representative lines from the two haplotypes. The results show that the mRNA abundance of *ZmNAET1* in HUANGC is higher than that in HZS. In contrast, the pre-mRNA of *ZmNAET1* in HUANGC accumulates much less than in HZS, suggesting that the splicing rate of Hap2 *ZmNAET1* is significantly slower than that of Hap1 *ZmNAET1*. Leveraging the traceable design of the CUBIC population, we identified two multi-parent recombinant inbred lines (RILs), MG_1054 and MG_1212, which share 76.6% genetic background identity but contain the Hap1 and Hap2 alleles of *ZmNAET1*, respectively. To further test whether the splicing rate variation is caused by *cis* elements, we crossed MG_1054 and MG_1212 (Figure S5A). In the F1 progeny, allele-specific expression analysis using haplotype-specific quantitative reverse-transcription primer pairs showed much higher mRNA but much lower pre-mRNA accumulation for Hap1 relative to Hap2 (Figures 1I, 1J, S5B, and S5C). All these data point to the conclusion that the high expression level of the Hap1 allele of *ZmNAET1* results from high splicing efficiency, most likely driven by the SNP or the SV in the second intron.

ZmNAET1 specifically controls the translocation of Ni to sink organs of maize

To confirm the function of *ZmNAET1* in controlling kernel Ni variation, we generated two knockout mutants (*crinaet1-1* and *crinaet1-2*) in the KN5585 background using CRISPR-Cas9 technology (Figure S6A) and isolated two independent ethyl methanesulfonate (EMS) mutant lines (*zmnaet1-1* and *zmnaet1-2*) in the B73 background (Figure S6B). These lines were planted in standard nursery fields in Shanghai and fertilized with urea as the main nitrogen fertilizer form. Elemental profile analysis showed that the Ni concentrations in the kernels of these mutants were reduced by 80% compared with those of the corresponding wild type (WT) (Figure 2A; Table S7). Allele

Please cite this article in press as: Chao et al., Nicotianamine-driven nickel transport to sink organs underpins maize productivity, Cell (2027), https://doi.org/10.1016/j.cell.2026.10.035

tests by crossing the two independent EMS mutants confirmed that the remarkable decrease in Ni concentration in the kernels is indeed controlled by *ZmNAET1* (Figure 2C). These data demonstrate that *ZmNAET1* is required for the accumulation of Ni in the kernels. We also generated two independent transgenic lines with a *pUbi::ZmNAET1-eYFP* construct that constitutively overexpresses *ZmNAET1* (Figure S7A). Consistently, the Ni concentrations in the kernels of the transgenic lines were significantly increased (Figure 2D; Table S7), further supporting that ZmNAET1 contributes to Ni loading into seeds.

In addition to kernels, the shoot apex of the *crinaet1* mutants also accumulated much less Ni than that of the WT (Figure 2E; Table S8), suggesting that *ZmNAET1* contributes to the transport of Ni to sink organs in general. Consistently, we observed that Ni concentrations in other sink organs, such as ears, tassels, and bracts of the mutants, were also significantly decreased, albeit to a lesser degree (Figure 2F; Table S8). In contrast, the Ni concentrations in the stem and nodes were significantly increased by the knockout of *ZmNAET1*, whereas those in adult leaves remained unaffected (Figure 2F). These data collectively demonstrate that *ZmNAET1* functions in the translocation of Ni from the nodes to the sink organs.

The orthologs of ZmNAET1 in *Arabidopsis*, AtNAET1, and AtNAET2 control the long-distance transport of Fe, Cu, and Co to the sink organs but not Ni or other elements.[20] Thus, we examined whether other elements, in addition to Ni, are affected by ZmNAET1. Surprisingly, we found that among all the tested metal elements, only Zn, aside from Ni, was affected by ZmNAET1, although the effect was very weak (Figures 2B, 2G, S4, and S8). These findings indicate that the metals regulated by ZmNAET1 are confined to Ni and Zn.

The role of NAET1 is conserved in graminaceous plants

To address whether the role of NAET1 is conserved in graminaceous plants, we identified two homologous proteins of ZmNAET1 in rice, namely, OsNAET1 and OsNAET2 (Figure S2). We generated single and double knockout mutants for these two genes in the Nipponbare background using CRISPR-Cas9 technology (Figures S9E). The two double mutants exhibit a remarkably lower Ni concentration in seeds compared with the WT or the single mutants (Figure S9F; Table S9), indicating that OsNAET1 and OsNAET2 are functionally redundant and essential for Ni accumulation in rice seeds. Consistently, OsNAET1 and OsNAET2 did not affect Fe and Co levels but slightly increased Zn and Cu in the seeds (Figure S9F), corroborating that the role of NAET1 is conserved in graminaceous plants. Conversely, in *Arabidopsis*, AtNAET1 and AtNAET2 have been shown to mediate NA secretion to the xylem and the apoplastic space of the phloem to facilitate the long-distance transport of Fe, Cu, and Co.[20] Thus, the distinct impact on metal allocation in different plant species may reflect a functional divergence of either NAET transporters or the subsequently formed NA chelates between graminaceous and nongraminaceous plants.

ZmNAET1 functions as a NAET

To test whether ZmNAET1 functions as a NAET, we generated stable transgenic lines expressing *pAtNAET2::ZmNAET1* in the *Arabidopsis naet1naet2* double mutant. Phenotyping of the transgenic lines showed that the expression of *ZmNAET1* driven by the promoter of *AtNAET2* can complement the defects of *naet1naet2* in ionomic and developmental phenotypes (Figures 3A–3C and S10; Table S10), indicating that ZmNAET1 functions as a NAET. To further validate these findings, we co-expressed *ZmNAET1* and the *AhNAS3* gene encoding NA synthase in the yeast strain NMY51. The results showed that the expression of ZmNAET1 led to a significant secretion of NA into the medium and a remarkable reduction in the cellular NA concentration (Figure 3D), confirming that ZmNAET1 functions as a NAET.

Consistent with the subcellular localization of AtNAET1/2,[20] ZmNAET1 also localized in dot-like structures in the cytoplasm of *Arabidopsis* mesophyll protoplasts (Figure 3E). Likewise, in transgenic lines expressing *pUbi::ZmNAET1-eYFP*, ZmNAET1 was detected in brefeldin A (BFA)-sensitive compartments (Figure S11A). Co-expression of ZmNAET1-GFP and AtNAET2-mCherry in the leaf epidermal cells of *Nicotiana benthamiana* showed that ZmNAET1 and AtNAET2 are indeed co-localized in the same type of secretory vesicles (Figure 3F). We also performed an immunofluorescence assay in transgenic lines expressing *pUbi::ZmNAET1-eYFP* using a specific anti-NA antibody and observed that intracellular NA compartments overlapped with the vesicles where ZmNAET1-eYFP was localized (Figures 3G and S11B). These data further support that ZmNAET1 functions in accumulating NA in secretory vesicles for NA secretion out of the cell.

ZmNAET1 mediates NA secretion to node phloem apoplast to facilitate Ni translocation to sink organs

To elucidate how ZmNAET1 controls the translocation of Ni, we investigated the expression patterns of *ZmNAET1*. According to RT-qPCR and RNA-seq results, *ZmNAET1* is mainly expressed in the stems and the shank, especially at the developing stage 30 days after pollination (DAP) (Figures 1F and S3C). Based on a β-glucuronidase (GUS) reporter driven by the *ZmNAET1* promoter, we found that *ZmNAET1* is predominantly expressed in the nodes of the stem and the shank (Figures 3H and 3I). Cross sections of shank nodes showed that *ZmNAET1* is mainly expressed in the phloem cells of nodes (Figure 3I). The specific expression of *ZmNAET1* indicates that the ZmNAET1-mediated NA secretion predominantly occurs in the node phloem to facilitate subsequent Ni translocation to sink organs. Consistent with this conclusion, we found that Ni concentrations in the nodes of *crinaet1* mutants were 55% higher than those in the WT (Figure 2F). These results reveal that ZmNAET1 controls the translocation of Ni from nodes to sink organs, including kernels, by mediating NA secretion from phloem cells. In the apoplastic space of the phloem, NA chelates free Ni to form Ni-NA complexes, which are subsequently imported into phloem cells by as yet unknown transporters for allocation to sink organs.

The detected expression patterns of *ZmNAET1* in maize (Figures 1F, 3H, 3I, and S3C) differ significantly from those of *AtNAET1* and *AtNAET2* in *Arabidopsis*[20]; we thus hypothesized that tissue-specific localization determines the dominant roles of NAETs in metal homeostasis between graminaceous and nongraminaceous plants. When we constitutively overexpressed *ZmNAET1* in maize, the long-distance transport of not only Ni

Please cite this article in press as: Chao et al., Nicotianamine-driven nickel transport to sink organs underpins maize productivity, Cell (2027), https://doi.org/10.1016/j.cell.2026.10.035

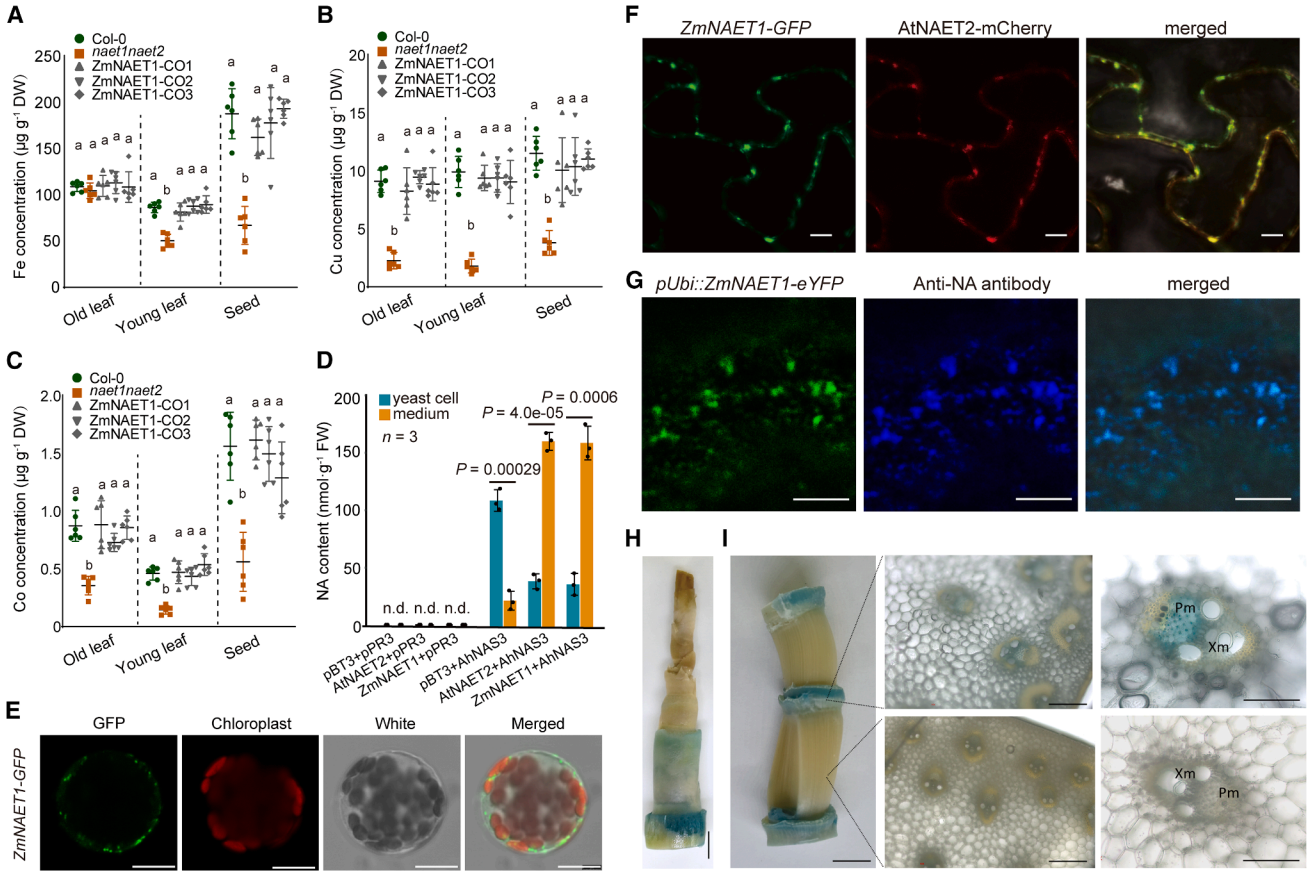


Figure 3. ZmNAET1 functions as an NA efflux transporter

(A–C) Concentrations of Fe (A), Cu (B) and Co (C) in different organs of the *Arabidopsis naet1naet2* mutant expressing *ZmNAET1*. CO1, CO2 and CO3 represent three independent transgenic lines of *naet1naet2* transformed with *pAtNAET2::ZmNAET1*.

(D) ZmNAET1 functions as an NAET in yeast cells. The yeast strain NMY51A was transformed with different constructs expressing *AhNAS3* and/or *ZmNAET1*. Yeast strains expressing empty vectors were used as negative controls, while the strain expressing *AtNAET2* and *AhNAS3* served as a positive control. NA amounts retained in yeast cells and secreted into the medium were detected using ultra-performance liquid chromatography-mass spec (UPLC-MS). n.d., not detectable.

(E) Subcellular localization of ZmNAET1 revealed by transient expression of *ZmNAET1-GFP* in Arabidopsis mesophyll protoplasts. Scale bar, 20 μm.

(F) Colocalization of ZmNAET1-GFP with AtNAET2-mCherry in leaf epidermal cells of *N. benthamiana*. Scale bar, 10 μm.

(G) Colocalization of ZmNAET1 with NA in vesicles. Immunostaining with an anti-NA antibody was performed in leaf epidermal cells of the transgenic lines expressing *pUbi::ZmNAET1-eYFP*. Images are representative of three independent lines. Fluorescence from the secondary antibody (purple) and YFP (green) is shown. Scale bar, 10 μm.

(H and I) Representative images of GUS-stained stems (H) and fruit stalks (I) expressing *pZmNAET1::GUS* in the KN5585 background (n = 3 independent transgenic lines).

Scale bars: 1 cm for (G) and the left panel of (H); 100 μm for the middle and right panel of (I). Cross sections of nodes and internodes are shown in the right panel. Pm, phloem; Xm, xylem. Bars represent means ± SD (n = 6 independent plants in (A–C) and n = 3 independent samples in D). Different letters indicate significant differences in the same group ($p < 0.05$), as determined by one-way ANOVA followed by Tukey's post hoc test (A–C). Statistical significance was determined by two-sided Student's t test (D).

and Zn but also Co and Cu to sink organs was significantly increased (Figures S7B–S7F). These results support that the expression of *ZmNAET1* in different tissues also alters the translocation of other metal ions to sink organs.

Ni and ZmNAET1 are essential for amino acid metabolism during germination

A time-course experiment up to 72 h showed that the germination speed of freshly harvested *crinaet1* seeds was much slower than that of freshly harvested WT seeds (Figures 4A and 4B). Interestingly, we found that the germination rate of the *crinaet1* seeds aged for 8 months or 1 year was remarkably lower compared with the WT seeds stored under the same conditions, whereas the germination rate of freshly harvested *crinaet1* seeds was comparable to that of the WT seeds (Figures 4C and 4D). These data demonstrate a role of ZmNAET1 in seed vigor and longevity.

The low Ni level in *zmneat1* seeds led us to propose that Ni is required for seed longevity in maize. To confirm this hypothesis, we applied different concentrations of Ni to the aged seeds

Please cite this article in press as: Chao et al., Nicotianamine-driven nickel transport to sink organs underpins maize productivity, Cell (2027), https://doi.org/10.1016/j.cell.2026.10.035

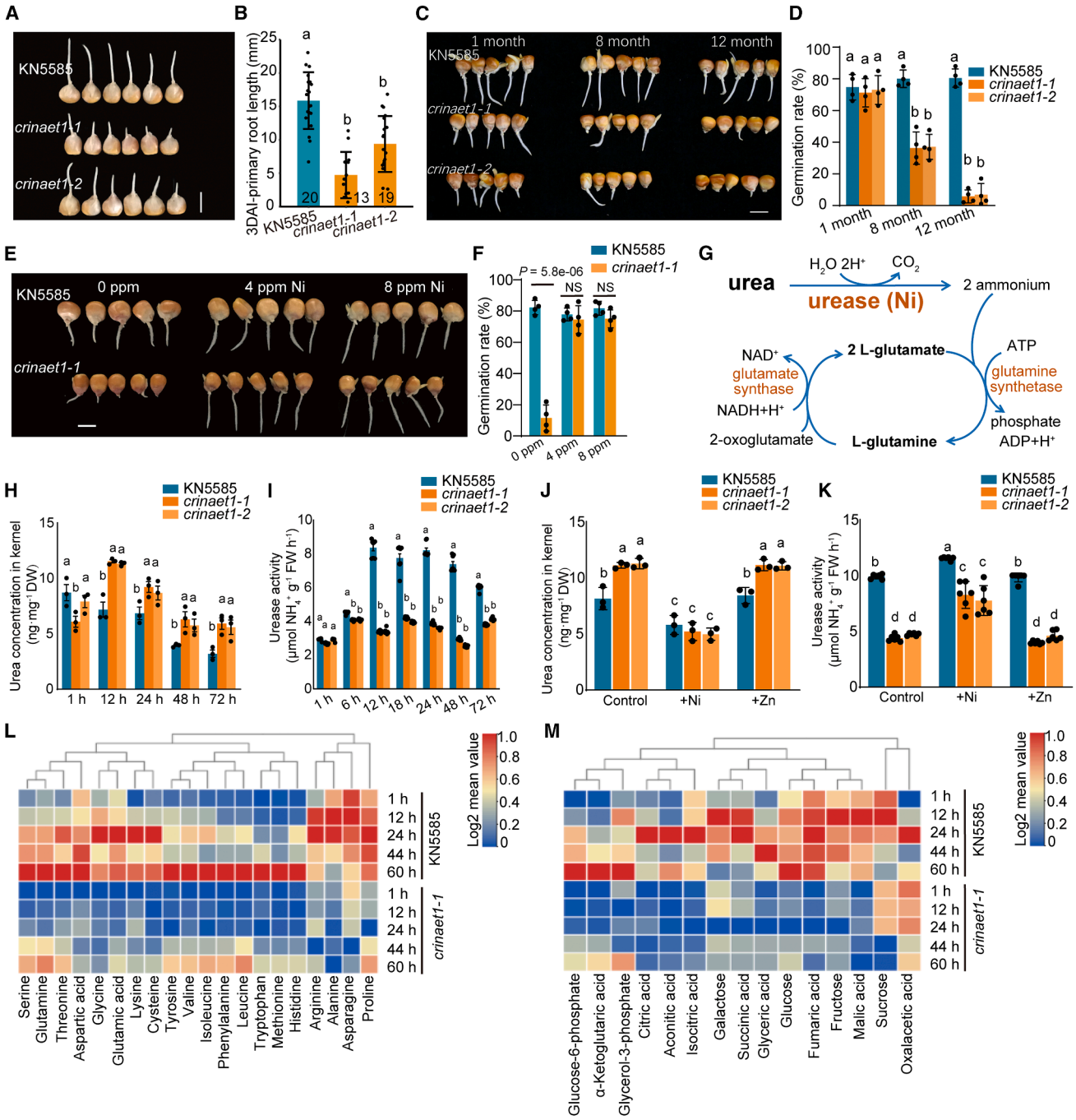


Figure 4. Ni is essential for urea N reutilization during seed germination

(A) Representative images of germinating seeds of KN5585 and *crinaet1* mutants. The experiment was performed using freshly harvested seeds stored for less than 1 month. Scale bar, 1 cm. Images were taken 3 days after 12 h of imbibition.

(B) Primary root length of the germinating seeds shown in (A). DAI, days after imbibition. Bars represent the means ± SD. Sample numbers are indicated in the corresponding columns.

(C) Representative images of seed germination after different storage periods. Scale bar, 1 cm. Images were taken 3 days after 12 h imbibition.

(D) Germination rates of the seeds shown in (C). Bars represent the means ± SD. *n* = 4 independent experiments, with 20 seeds per replicate.

(E) Representative images of seed germination under Ni treatment at different concentrations. The seeds used had been stored for 1 year. Scale bar, 1 cm. Images were taken 3 days after 12 h of imbibition.

(F) Germination rates of the seeds shown in (E). Bars represent the means ± SD. *n* = 4 independent experiments, with 20 seeds per replicate.

(legend continued on next page)

Please cite this article in press as: Chao et al., Nicotianamine-driven nickel transport to sink organs underpins maize productivity, Cell (2027), https://doi.org/10.1016/j.cell.2026.10.035

during germination and found that supplementation of 4 ppm Ni^{2+} could efficiently rescue the germination rate and germination speed phenotypes of the *crinaet1* mutants (Figures 4E and 4F; Table S11). In contrast, the addition of different concentrations of Zn^{2+} could not rescue these phenotypes, and high concentrations of Zn even inhibited seed germination (Figures S12A and S12B). These data indicate that ZmNAET1 contributes to seed longevity by ensuring sufficient Ni accumulation in the seeds.

Ni is a cofactor of urease required for amino acid metabolism[7,22] (Figure 4G). As amino acid metabolism is essential during seed germination, we hypothesized that the involvement of ZmNAET1 in seed germination is related to the Ni requirement of urease and urea hydrolysis. To test this hypothesis, we determined the urea concentrations and urease activity in the mutants and WT during seed germination (Table S12). As expected, urea indeed accumulated in the mutants during germination (Figure 4H). Consistently, we found that urease activity was significantly impaired in the germinating mutant seeds, either calculated on a per-mass or per-protein basis (Figures 4I, S12E, and S12F). Interestingly, we also observed that urease activity in WT tended to increase during germination, further supporting that urease activity is required for seed germination. Ni supply fully rescued the over-accumulation of urea and partially restored urease activity in the mutants, irrespective of whether calculated on a per-mass or per-kernel basis (Figures 4J, 4K, and S12C–S12F; Table S12). In contrast, such effects were not observed with Zn supplementation (Figures 4J, 4K, and S12C–S12F). These results demonstrate that the requirement of ZmNAET1 for seed germination is due to the role of Ni in maintaining urease activity for urea hydrolysis.

To further examine the impact of ZmNAET1 and Ni on metabolism during seed germination, we further analyzed metabolite profiles of germinating seeds of the freshly harvested *crinaet1-1* mutant and WT (Figures 4L and 4M; Table S13). Given that ammonia released by urease hydrolysis is assimilated through glutamine and glutamate (Figure 4G), we focused on these two metabolites as key indicators of nitrogen assimilation. During germination, the contents of free glutamine and glutamic acid, along with several other amino acids, dramatically increased in WT seeds, whereas this increase was not evident in the mutant seeds (Figure 4L), suggesting that amino acid metabolism is impaired in the mutants. Glutamine and glutamic acid generally serve as amino group donors to sustain synthesis of other amino acids and carbon skeletons in the tricarboxylic acid (TCA) cycle.[23,24] Consistently, during germination, the concentrations of most amino acids (Figure 4L) and TCA cycle components did not increase in the mutant seeds as they did in the WT seeds (Figure 4M), indicating that N and C metabolism was impaired in *crinaet1* mutants. Growth inhibition of the *zmnaet1-1* mutants was also observed in Ni-free hydroponic conditions at the seedling growth stage (Figure S13), indicating that N and C starvation in germinating *crinaet1* seeds not only slows down the germination speed but also hinders subsequent seedling development in Ni-free conditions.

Ni homeostasis controlled by *ZmNAET1* is required for urea hydrolysis in sink organs

To further investigate the physiological role of *ZmNAET1* and Ni in field-grown maize, we compared agronomic traits between mutant and WT maize when fertilized with urea as the main nitrogen fertilizer form. We observed that the plant height of the mutants (*crinaet1-1*, *crinaet1-2*, *zmnaet1-1*, and *zmnaet1-2*) at flowering was significantly lower than that of the WTs (Figures 5A, 5C, S14A, and S14B), and this height difference was only observed at 4 weeks post-germination (Figure S15A). Further analysis showed that the lower plant height of the mutants resulted from both fewer nodes and shorter internode lengths (Figures S15B and S15C). In addition to plant height, the ear weight, starch content, and grain size were significantly affected by the mutation of *ZmNAET1* (Figures 5B, 5D, S14C, S14D, and S15D–S15G). The average ear weights of the *crinaet1* and *zmnaet1* mutants were reduced to 78% and 51%, respectively, compared with the corresponding WT (Figures 5B, 5D, S14D, and S14E). These results demonstrate that ZmNAET1 and Ni are essential for plant fitness in both vegetative and reproductive growth and the development of maize.

To investigate the mechanism by which ZmNAET1 regulates these agronomic traits, we first determined N concentrations in different tissues. In most of the tissues, N concentrations did not significantly differ between *crinaet1* mutants and WT, but in the shoot apex of *crinaet1* plants, N concentrations were 51% lower than in the WT (Figure 5E; Table S14), suggesting an impaired N translocation into the shoot apex in the mutants, probably as a result of feedback regulation. As Ni is a cofactor of urease required for urea hydrolysis, we then checked the

(G) Diagrams of urease-catalyzed conversion of urea to ammonia and bicarbonate. The released ammonium is subsequently reassimilated into glutamine and glutamate by the corresponding enzymes. Glutamine and glutamate also serve as amino group donors to sustain the synthesis of amino acids and TCA cycle metabolites.

(H) Urea content in kernels of *crinaet1* mutants and KN5585 during seed germination. Bars represent the means ± SD. $n = 3$ independent samples. Seeds harvested from different ears were used for analysis.

(I) Urease activity in kernels of *crinaet1* mutants and KN5585 during seed germination. Bars represent the means ± SD. $n = 7$. Seeds harvested from different ears were used for analysis.

(J) Urea content in kernels of *crinaet1* mutants and KN5585 during seed germination with or without Ni or Zn after 12 h of imbibition. Bars represent the means ± SD. $n = 3$. Seeds harvested from different ears were used for analysis.

(K) Urease activity in kernels of *crinaet1* mutants and KN5585 during seed germination with or without Ni or Zn after 12 h of imbibition. Bars represent the means ± SD. $n = 6$. Seeds harvested from different ears were used for analysis. During the 12 h imbibition period, 68 μM Ni or 50 μM Zn were used in (J) and (K).

(L and M) Profiles of amino acids (L) and metabolites in TCA cycle (M) of *crinaet1-1* mutant and KN5585 during seed germination. The unit is ng mg^{-1} DW.

Statistical significance in (F) was determined by two-sided Student's *t* test (NS, not significant). Different letters indicate significant differences in the same group ($p < 0.05$), as determined by one-way ANOVA followed by Tukey's post hoc test (B, D, H, and I). Statistical significance was assessed by two-way ANOVA followed by Tukey's multiple comparisons test (J and K).

Please cite this article in press as: Chao et al., Nicotianamine-driven nickel transport to sink organs underpins maize productivity, Cell (2027), https://doi.org/10.1016/j.cell.2026.10.035

CellPress

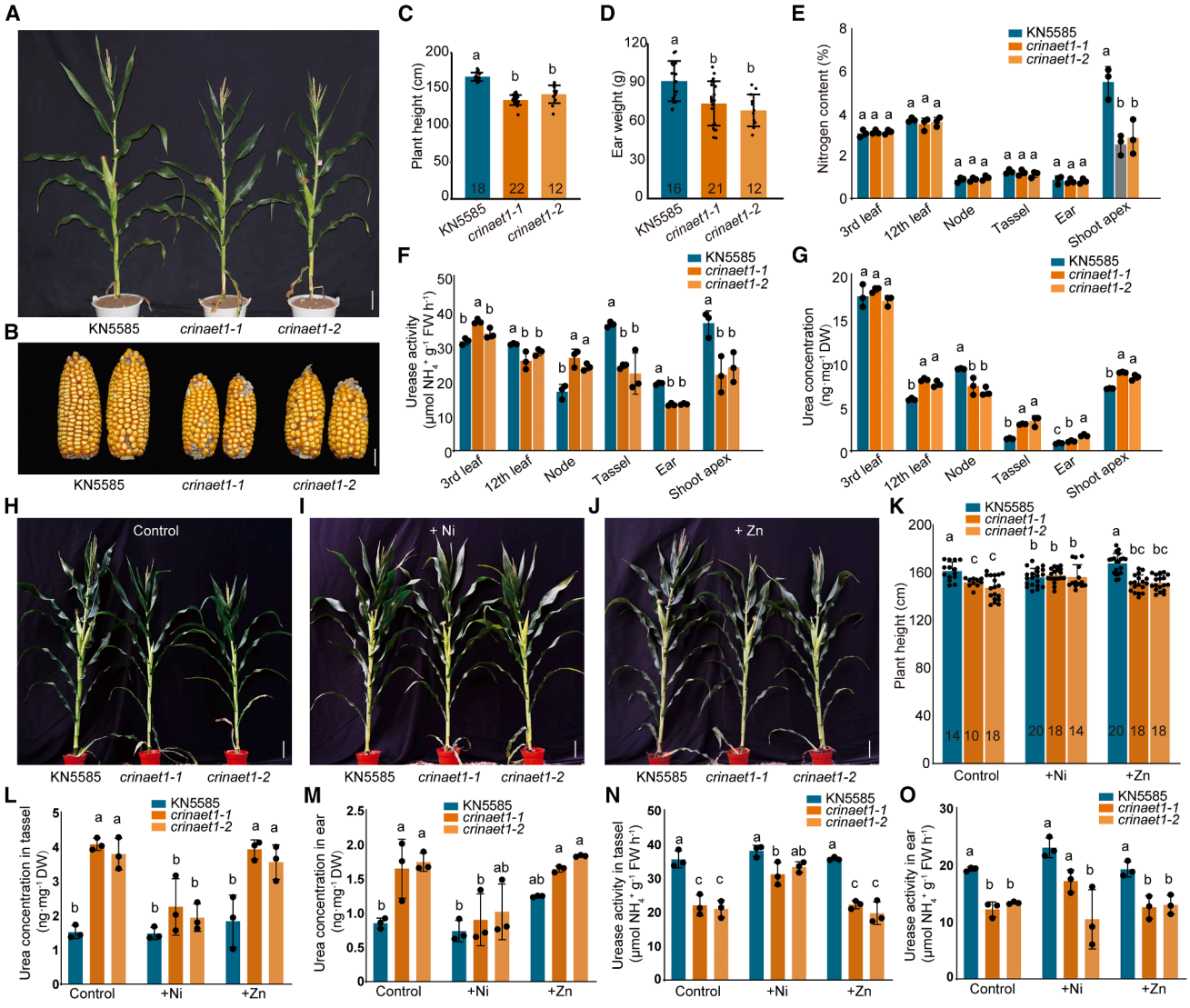


Figure 5. Ni and ZmNAET1 contribute to shoot growth

(A) Representative images of the *crinaet1* mutants and the WT (KN5585) at the flowering stage (n = 5 independent experiments). Plants were grown in the field, then dug out and placed in pots for photography.

(B) Representative images of ears of independent *crinaet1* mutants and corresponding WT grown in the field (n = 5 independent experiments). Images were taken 9 weeks after germination, during the reproductive stage after pollination.

(C and D) Plant height (C) and ear weight (D) of *crinaet1* mutants and the WT. Bars represent means ± SD.

(E) Total nitrogen content in the 3rd leaf, 12th leaf, node, tassel, ear, and shoot apex of *crinaet1* mutants and KN5585. Bars represent means ± SD (n = 3 biologically independent samples from different plants).

(F) Urease activity in the 3rd leaf, 12th leaf, node, tassel, ear, and shoot apex of *crinaet1* mutants and KN5585. Bars represent the means ± SD. n = 3 independent samples.

(G) Urea content in the 3rd leaf, 12th leaf, node, tassel, ear, and shoot apex of *crinaet1* mutants and KN5585. Bars represent the means ± SDs. n = 3 independent samples.

(H–J) Representative images of *crinaet1* mutants and KN5585 grown in the field and sprayed with water (H), 5 μM $NiSO_4$ (I) and 460 μM $ZnSO_4$ (J). The pictures were taken 9 weeks after germination, during the reproductive stage after pollination.

(K) Plant height of *crinaet1* mutants and KN5585 grown in the field under control, Ni-spray, and Zn-spray conditions. Bars represent means ± SD. The numbers of plants are indicated in the corresponding column.

(L and M) Urea content in tassel (L) and ear (M) of *crinaet1* mutants and KN5585 with or without Ni or Zn spraying during plant development. Bars represent the means ± SD. n = 3 independent samples from different plants.

(N and O) Urease activity in tassel (N) and ear (O) of *crinaet1* mutants and KN5585 during seed germination with or without Ni or Zn spraying during plant development. The solutions were sprayed once a week after germination. Bars represent the means ± SD. n = 3 independent samples from different plants.

Scale bar: 15 cm in (A) and (H–J); 2 cm in (B). Different letters indicate significant differences in the same group ($p < 0.05$), as determined by one-way ANOVA followed by Tukey's post hoc test (C–G). Statistical significance was assessed by two-way ANOVA followed by Tukey's multiple comparisons test (K–O).

Please cite this article in press as: Chao et al., Nicotianamine-driven nickel transport to sink organs underpins maize productivity, Cell (2027), https://doi.org/10.1016/j.cell.2026.10.035

urease activity in different tissues (Table S12). The urease activity in the shoot apex, young leaf, ear, and tassel of the *crinaet1* mutants was much less than that of the WT (Figure 5F). In contrast, the urease activity in the nodes was significantly increased in *crinaet1* mutants, whereas it remained unaffected in adult leaves (Figure 5F). These results indicate that urea hydrolysis in *crinaet1* mutants is also impaired in sink organs, at least in the tissues measured, implying an essential role of Ni in sink organ development. We then found that the decreases in urease activity were paralleled by an increase in the urea concentration in sink organs, especially in the shoot apex, young leaf, ear, and tassel (Figure 5G). In addition, the glutamic acid and glutamine concentrations in the shoot apex, tassel, and mature kernels of *crinaet1* mutants were remarkably lower than in the WT but higher in nodes (Figures S15H and S15I; Table S12). These data collectively demonstrated that urease activity in the mutants was not sufficient to cope with internal urea accumulation in developing sink organs due to the lack of Ni.

To validate whether the changes in these agronomic traits in *crinaet1* mutants were caused by a Ni or Zn defect, we performed a chemical complementation test in the field (Figures 5H–5O and S16). By spraying with either Ni or Zn, we found that Ni fully rescued the plant height of *crinaet1* mutants, whereas Zn supply remarkably increased the plant height of the WT rather than of *crinaet1* mutants (Figures 5H–5K). This clearly indicated that the decrease in plant height in *crinaet1* mutants resulted from Ni deficiency. Next, we collected sink organs, such as developing tassels and ears, to assess their ionome, as well as urea and amino acid concentrations and urease activities. These tissues were enclosed by leaves and thus not directly exposed to the foliar spray, minimizing the risk of contamination. Following the spray, we observed a corresponding increase in Ni or Zn concentration in sink organs of both mutant and WT plants (Figures S16A–S16D). Under Zn treatment, Zn concentrations in *zmnaet1* mutants were comparable to those in the WT. In contrast, under Ni treatment, Ni concentrations in *zmnaet1* mutants remained lower than in the WT; however, they were higher than or comparable to those observed in untreated WT plants, indicating that this partial increase in Ni is sufficient to complement the Ni-deficiency phenotype in the mutants. Additionally, under Ni supply, comparable urea concentrations were measured in the sink organs of *crinaet1* mutant and WT plants (Figures 5L and 5M; Table S12). In contrast, urease activity, glutamic acid, and glutamine tended to increase in the sink organs under Ni supply (Figures 5N, 5O, and S16E–S16H), whereas a similar effect was not seen with Zn supply. These observations showed that Ni translocation controlled by *ZmNAET1* is required for nitrogen metabolism and subsequent yield formation in sink organs.

DISCUSSION

Ni is the most recently identified essential element for plants.[3–5] However, the genetic and molecular mechanisms underlying Ni homeostasis in plants, particularly in crops, have remained poorly understood. This knowledge gap has strongly restricted our understanding of the role of this micronutrient in plant biology, hindering its targeted exploitation toward optimized yield and agricultural traits.

In this study, we identified the first gene controlling the long-distance translocation of Ni in graminaceous plants, providing unprecedented insights into the genetic basis of Ni homeostasis in sink organs and highlighting the critical role of Ni in the agricultural production of crops. Our data revealed that ZmNAET1 contributes to Ni translocation by mediating NA secretion to the apoplast of the node phloem cells. We propose that, once synthesized, NA is transported into vesicles by NAET1 before it is secreted out of the cells via exocytosis. In the apoplast, NA chelates divalent metals, in particular Ni, forming Ni-NA complexes that are then re-imported into phloem cells by one or more transporters distinct from NAET1, thereby facilitating their long-distance translocation toward sink organs (Figure 6). Our research further shows that the loss of ZmNAET1 function results in low Ni levels and disrupted urease activity in developing sink organs. As Ni acts as a cofactor for urease,[6] impaired urea hydrolysis results in less fuel for amino acid metabolism in germinating seeds and in developing shoot organs, where amino acid turnover is particularly high. Thus, the characterization of ZmNAET1 offers a new perspective for further exploration of the physiological relevance of Ni and its regulatory factors.

In general, the plant demand for Ni is low, and it is thus thought that Ni deficiency is rare in agriculture. The present study shows that this perspective fails to consider the natural variations in Ni utilization efficiency among crops and, due to an underestimation of Ni's physiological impact, does not correspond to a comprehensive understanding of Ni deficiency. In the literature, graminaceous plants (e.g., barley and maize) are believed to require rather low Ni levels, approximately 0.05 to 0.1 $\mu g\ g^{-1}$ DW.[25] Nevertheless, despite this relatively low overall requirement, Ni transport to the seeds appears to be essential, at least in barley.[4] In contrast, nongraminaceous species, including Brassicaceae and in particular legumes, have a higher demand for Ni, with up to 4.3 $\mu g\ g^{-1}$ in soybean.[25,26] Legumes are highly sensitive to Ni deficiency as nitrogen fixation into ureides requires high urease activities for nitrogen metabolism.[25] Our study in maize revealed that the high demand for Ni goes beyond its known role in seeds but applies to developing sink organs, where amino acid turnover rates are high and Ni provision is likely an underestimated nutritional problem.

Despite the great importance of urea as a major nitrogen fertilizer form for crops, the importance of urea hydrolysis in developing sink organs is not yet recognized.[27,28] So far, urea has been characterized as a short-lived metabolic marker in cotyledons of germinated seedlings and senescing leaves,[29,30] and urease activities have been considered sufficient to cope with internally produced urea in graminaceous and nongraminaceous species.[28,29] Our results in maize, however, overturn this assumption, revealing a substantially higher Ni requirement to sustain urease activity in developing shoot organs. During organ development, amino acid import and turnover are very high, obviously requiring the hydrolysis of urea released from arginine decomposition. Hence, Ni-dependent urease is required to efficiently break down urea and release ammonia for *de novo* ammonium assimilation. Currently, it is unclear which allelic variants of NAETs exist in the major elite cultivars of cereal crops and whether they cause a hidden undersupply of Ni in developing shoot organs. Future studies should thus explore Ni provision in sinks and revisit critical Ni deficiency levels in cereal crops.

Please cite this article in press as: Chao et al., Nicotianamine-driven nickel transport to sink organs underpins maize productivity, Cell (2027), https://doi.org/10.1016/j.cell.2026.10.035

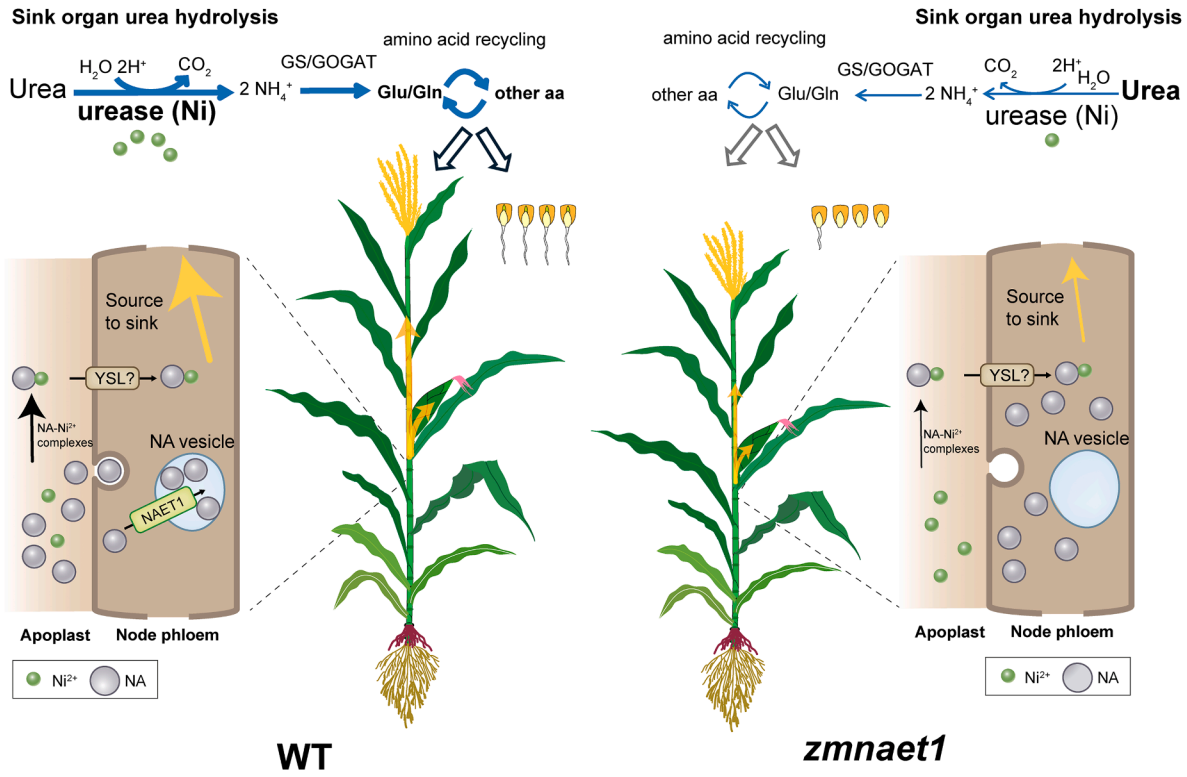


Figure 6. Proposed working model of ZmNAET1-mediated Ni transport and utilization in maize

Phloem cells in maize nodes express ZmNAET1 to mediate secretion of cytosolically synthesized NA into the apoplastic space to form NA-Ni^{2+} complexes. These complexes can be re-imported into phloem cells by yet unidentified transporters, possibly YSL (yellow stripe 1-like) proteins, for the long-distance transport to sink organs. In developing shoot organs and germinating seeds, where amino acid turnover is particularly high, Ni acts as a cofactor for urease to facilitate urea hydrolysis and amino acid metabolism. Through this essential role, Ni contributes to seed vigor, plant height, and crop productivity. The green balls indicate Ni^{2+} and the gray balls indicate NA.

As an important intermediate of mugineic acid (MAs) biosynthesis in graminaceous plants, NA has been reported to function as a key metal chelator for intracellular metal trafficking and long-distance metal transport in nongraminaceous plants,[12,13] e.g., facilitating Fe and Cu transport into seeds of *Arabidopsis*.[20] However, the function of NA in graminaceous plants has remained largely unclear. In rice, the NAETs OsENA1/2 have been proposed to be responsible for NA transport out of cells,[31] but knockout or overexpression of *OsENA1* did not result in any phenotype related to Fe,[32] which raised the question of the exact roles of OsENA1 and NA in graminaceous plants. Our evidence in maize and rice suggests that the primary function of NA, aside from serving as a precursor to MAs, is to facilitate Ni and Zn translocation to sink organs in graminaceous plants. The efficiency of NA-mediated metal translocation may be further modulated by species- and tissue-specific factors, including NAET1 ortholog expression patterns, pH environments in xylem and phloem, concentrations of micronutrients, and the presence of competing micronutrient chelators, such as citrate and MAs.[33] In graminaceous plants, nutrient distribution is additionally regulated by a specialized nodal plexus that forms an interconnected vascular hub absent in dicots.

Altogether, our detailed characterization of NAETs thus uncovers a previously underappreciated requirement for NA and Ni in cereal crop productivity and opens a new research avenue toward optimizing micronutrient provision in cereal crop species by selecting favorable allelic variants of NAETs.

Limitations of the study

Although the phenotypes associated with NAET1 perturbation are largely attributable to altered Ni availability and urease activity, contributions from other, yet unidentified Ni-requiring enzymes cannot be excluded. Given the ability of NA to chelate multiple transition metals, NAET1 may also influence the homeostasis of metals beyond Ni, although its effects on Ni homeostasis were the strongest and most consistent in our study. The mechanism underlying the transcriptional regulation of NAET1 remains to be further elucidated. The relevance of Ni homeostasis in other crop species also remains to be determined.

RESOURCE AVAILABILITY

Lead contact

Further information and requests for resources and reagents should be directed to and will be fulfilled by the lead contact, Dai-Yin Chao (dychao@cemps.ac.cn).

Materials availability

Plasmids, transgenic plants, and unique/stable reagents generated in this study will be made available on request for scientific research, but we may require payment and a complete materials transfer agreement for commercial purposes.

Data and code availability

- All data are available in the main text and supplemental information or at public databases. The SNPs and bins of the CUBIC population can be downloaded from http://cubicmaize.hzau.edu.cn/Magic/download/download.jsp.
- This study does not report original code.
- Any additional information required to reanalyze the data reported in this study is available from the lead contact or Jianbing Yan (yjianbing@mail.hzau.edu.cn) upon request.

ACKNOWLEDGMENTS

We thank Dr. Peng Yu from the Technical University of Munich (TUM) and Dr. Ricardo F.H. Giehl from IPK for their critical reading and suggestions on the manuscript. We thank Hao Liu from Huazhong Agricultural University for help in managing the high-throughput computing system. We thank Shanshan Wang and Lianyan Jing from the CAS Center for Excellence in Molecular Plant Sciences (CEMPS) for their help in detecting NA and urea content. We thank Yuanyuan Gao in CEMPS for help with amino acid measurement. We thank Dr. Yidong Zhu and Prof. Yongrui Wu in CEMPS for their help with N measurement. This research was supported by the Strategic Priority Research Program of the Chinese Academy of Sciences (XDB1490000), the Biological Breeding-National Science and Technology Major Project (2023ZD04071), the National Natural Science Foundation of China (32321005 and W2511029), the Science and Technology Major Program of Hubei Province (2021ABA011), and the 111 Project Crop Genomics and Molecular Breeding (B20051).

AUTHOR CONTRIBUTIONS

D.-Y.C. and J.Y. designed and supervised this study. Z.-F.C., Y.C., J.-C.W., and X.W. performed the field trials. J.-C.W. performed the field chemical complementation tests. Y.C., H.-J.L., and Y.X. performed the GWAS data analysis. Y.-L.W., Z.-F.C., J.-C.W., and M.-L.H. collected ICP-MS data. Z.-F.C., J.-C.W., Y.C., and L.-Y.F. carried out validation of gene function analysis. Y.P. performed the RNA-seq analysis. Z.-F.C., Y.C., and D.-Y.C. wrote the manuscript. D.-Y.C., J.Y., and N.V.W. revised and completed the manuscript. All authors have seen and approved the final version of the manuscript submitted.

DECLARATION OF INTERESTS

The authors have a patent application and/or registration related to this work.

STAR★METHODS

Detailed methods are provided in the online version of this paper and include the following:

- KEY RESOURCES TABLE
- EXPERIMENTAL MODEL AND STUDY PARTICIPANT DETAILS
  - Plant materials and growth conditions
- METHOD DETAILS
  - Elemental profiling
  - Genome-wide association study
  - LD analysis and QTL definition
  - RNA-Seq and RT-qPCR analysis
  - Vector construction and plant transformation
  - Yeast expression and NA detection
  - Immunostaining of NA
  - Cell imaging
  - Phylogeny analysis
  - Measurement of N, protein and starch
  - Urea and amino acids detection
  - Detection of urease activity
  - GC-MS
- QUANTIFICATION AND STATISTICAL ANALYSIS

SUPPLEMENTAL INFORMATION

Supplemental information can be found online at https://doi.org/10.1016/j.cell.2026.10.035.

Received: February 25, 2025
Revised: May 28, 2026
Accepted: October 20, 2026

REFERENCES

1. von Liebig, J. (1840). Die organische Chemie in ihrer Anwendung auf Agricultur und Physiologie (Springer Nature). https://doi.org/10.1007/978-3-662-62150-9.
2. Roach, W.A., and Barclay, C. (1946). Nickel and multiple trace element deficiencies in agricultural crops. Nature *157*, 696. https://doi.org/10.1038/157696a0.
3. Eskew, D.L., Welch, R.M., and Norvell, W.A. (1984). Nickel in higher plants: further evidence for an essential role. Plant Physiol. *76*, 691–693. https://doi.org/10.1104/pp.76.3.691.
4. Brown, P.H., Welch, R.M., and Cary, E.E. (1987). Nickel: a micronutrient essential for higher plants. Plant Physiol. *85*, 801–803. https://doi.org/10.1104/pp.85.3.801.
5. Eskew, D.L., Welch, R.M., and Cary, E.E. (1983). Nickel: an essential micronutrient for legumes and possibly all higher plants. Science *222*, 621–623. https://doi.org/10.1126/science.222.4624.621.
6. Dixon, N.E., Gazzola, T.C., Blakeley, R.L., and Zermer, B. (1975). Letter: jack bean urease (EC 3.5.1.5). A metalloenzyme. A simple biological role for nickel? J. Am. Chem. Soc. *97*, 4131–4133. https://doi.org/10.1021/ja00847a045.
7. Jabri, E., Carr, M.B., Hausinger, R.P., and Karplus, P.A. (1995). The crystal structure of urease from Klebsiella aerogenes. Science *268*, 998–1004. https://doi.org/10.1126/science.7754395.
8. Krämer, U., Cotter-Howells, J.D., Charnock, J.M., Baker, A.J.M., and Smith, J.A.C. (1996). Free histidine as a metal chelator in plants that accumulate nickel. Nature *379*, 635–638. https://doi.org/10.1038/379635a0.
9. Wycisk, K., Kim, E.J., Schroeder, J.I., and Krämer, U. (2004). Enhancing the first enzymatic step in the histidine biosynthesis pathway increases the free histidine pool and nickel tolerance in Arabidopsis thaliana. FEBS Lett. *578*, 128–134. https://doi.org/10.1016/j.febslet.2004.10.086.
10. Ingle, R.A., Mugford, S.T., Rees, J.D., Campbell, M.M., and Smith, J.A.C. (2005). Constitutively High Expression of the Histidine Biosynthetic Pathway Contributes to Nickel Tolerance in Hyperaccumulator Plants. Plant Cell *17*, 2089–2106. https://doi.org/10.1105/tpc.104.030577.
11. Shojima, S., Nishizawa, N.K., Fushiya, S., Nozoe, S., Irifune, T., and Mori, S. (1990). Biosynthesis of Phytosiderophores: In Vitro Biosynthesis of 2′-Deoxymugineic Acid from L-Methionine and Nicotianamine. Plant Physiol. *93*, 1497–1503. https://doi.org/10.1104/pp.93.4.1497.
12. Curie, C., Cassin, G., Couch, D., Divol, F., Higuchi, K., Le Jean, M., Misson, J., Schikora, A., Czernic, P., and Mari, S. (2009). Metal movement within the plant: contribution of nicotianamine and yellow stripe 1-like transporters. Ann. Bot. *103*, 1–11. https://doi.org/10.1093/aob/mcn207.
13. Chao, Z.-F., and Chao, D.-Y. (2024). Barriers and Carriers for Transition Metal Homeostasis in Plants. Plant Commun. *6*, 101235. https://doi.org/10.1016/j.xplc.2024.101235.
14. Mari, S., Gendre, D., Pianelli, K., Ouerdane, L., Lobinski, R., Briat, J.-F., Lebrun, M., and Czernic, P. (2006). Root-to-shoot long-distance

Please cite this article in press as: Chao et al., Nicotianamine-driven nickel transport to sink organs underpins maize productivity, Cell (2027), https://doi.org/10.1016/j.cell.2026.10.035

circulation of nicotianamine and nicotianamine–nickel chelates in the metal hyperaccumulator Thlaspi caerulescens. J. Exp. Bot. *57*, 4111–4122. https://doi.org/10.1093/jxb/erl184.

15. Shiferaw, B., Prasanna, B.M., Hellin, J., and Bänziger, M. (2011). Crops that feed the world 6. Past successes and future challenges to the role played by maize in global food security. Food Secur. *3*, 307–327. https://doi.org/10.1007/s12571-011-0140-5.
16. Erenstein, O., Jaleta, M., Sonder, K., Mottaleb, K., and Prasanna, B.M. (2022). Global maize production, consumption and trade: trends and R&D implications. Food Secur. *14*, 1295–1319. https://doi.org/10.1007/s12571-022-01288-7.
17. Polacco, J.C., Mazzafera, P., and Tezotto, T. (2013). Opinion – Nickel and urease in plants: Still many knowledge gaps. Plant Sci. *199–200*, 79–90. https://doi.org/10.1016/j.plantsci.2012.10.010.
18. Sweetlove, L.J., and Fernie, A.R. (2018). The role of dynamic enzyme assemblies and substrate channelling in metabolic regulation. Nat. Commun. *9*, 2136. https://doi.org/10.1038/s41467-018-04543-8.
19. Liu, H.-J., Wang, X., Xiao, Y., Luo, J., Qiao, F., Yang, W., Zhang, R., Meng, Y., Sun, J., Yan, S., et al. (2020). CUBIC: an atlas of genetic architecture promises directed maize improvement. Genome Biol. *21*, 20. https://doi.org/10.1186/s13059-020-1930-x.
20. Chao, Z.F., Wang, Y.L., Chen, Y.Y., Zhang, C.Y., Wang, P.Y., Song, T., Liu, C.B., Lv, Q.Y., Han, M.L., Wang, S.S., et al. (2021). NPF transporters in synaptic-like vesicles control delivery of iron and copper to seeds. Sci. Adv. *7*, eabh2450. https://doi.org/10.1126/sciadv.abh2450.
21. Chao, Z.F., and Chao, D.Y. (2022). Similarities and differences in iron homeostasis strategies between graminaceous and nongraminaceous plants. New Phytol. *236*, 1655–1660. https://doi.org/10.1111/nph.18482.
22. Allen, A.E., Dupont, C.L., Oborník, M., Horák, A., Nunes-Nesi, A., McCrow, J.P., Zheng, H., Johnson, D.A., Hu, H., Fernie, A.R., et al. (2011). Evolution and metabolic significance of the urea cycle in photosynthetic diatoms. Nature *473*, 203–207. https://doi.org/10.1038/nature10074.
23. Liao, H.-S., Chung, Y.-H., and Hsieh, M.-H. (2022). Glutamate: A multifunctional amino acid in plants. Plant Sci. *318*, 111238. https://doi.org/10.1016/j.plantsci.2022.111238.
24. Lam, H.M., Coschigano, K.T., Oliveira, I.C., Melo-Oliveira, R., and Coruzzi, G.M. (1996). The Molecular Genetics of Nitrogen Assimilation into Amino Acids in Higher Plants. Annu. Rev. Plant Physiol. Plant Mol. Biol. *47*, 569–593. https://doi.org/10.1146/annurev.arplant.47.1.569.
25. Shahzad, B., Tanveer, M., Rehman, A., Cheema, S.A., Fahad, S., Rehman, S., and Sharma, A. (2018). Nickel; whether toxic or essential for plants and environment - A review. Plant Physiol. Biochem. *132*, 641–651. https://doi.org/10.1016/j.plaphy.2018.10.014.
26. Arkoun, M., Jannin, L., Laîné, P., Etienne, P., Masclaux-Daubresse, C., Citerne, S., Garnica, M., Garcia-Mina, J.-M., Yvin, J.-C., and Ourry, A. (2013). A physiological and molecular study of the effects of nickel deficiency and phenylphosphorodiamidate (PPD) application on urea metabolism in oilseed rape (Brassica napus L.). Plant Soil *362*, 79–92. https://doi.org/10.1007/s11104-012-1227-2.
27. Bu, Y., Dong, X., Zhang, R., Shen, X., Liu, Y., Wang, S., Takano, T., and Liu, S. (2024). Unraveling the role of urea hydrolysis in salt stress response during seed germination and seedling growth in Arabidopsis thaliana. eLife *13*, e96797. https://doi.org/10.7554/eLife.96797.
28. Cao, F.Q., Werner, A.K., Dahncke, K., Romeis, T., Liu, L.H., and Witte, C.P. (2010). Identification and characterization of proteins involved in rice urea and arginine catabolism. Plant Physiol. *154*, 98–108. https://doi.org/10.1104/pp.110.160929.
29. Bohner, A., Kojima, S., Hajirezaei, M., Melzer, M., and von Wirén, N. (2015). Urea retranslocation from senescing Arabidopsis leaves is promoted by DUR3-mediated urea retrieval from leaf apoplast. Plant J. *81*, 377–387. https://doi.org/10.1111/tpj.12740.
30. Masclaux-Daubresse, C., Daniel-Vedele, F., Dechorgnat, J., Chardon, F., Gaufichon, L., and Suzuki, A. (2010). Nitrogen uptake, assimilation and remobilization in plants: challenges for sustainable and productive agriculture. Ann. Bot. *105*, 1141–1157. https://doi.org/10.1093/aob/mcq028.
31. Nozoye, T., Nagasaka, S., Kobayashi, T., Takahashi, M., Sato, Y., Sato, Y., Uozumi, N., Nakanishi, H., and Nishizawa, N.K. (2011). Phytosiderophore efflux transporters are crucial for iron acquisition in graminaceous plants. J. Biol. Chem. *286*, 5446–5454. https://doi.org/10.1074/jbc.M110.180026.
32. Nozoye, T., von Wirén, N., Sato, Y., Higashiyama, T., Nakanishi, H., and Nishizawa, N.K. (2019). Characterization of the Nicotianamine Exporter ENA1 in Rice. Front. Plant Sci. *10*, 502. https://doi.org/10.3389/fpls.2019.00502.
33. Rellán-Álvarez, R., Abadía, J., and Álvarez-Fernández, A. (2008). Formation of metal-nicotianamine complexes as affected by pH, ligand exchange with citrate and metal exchange. A study by electrospray ionization time-of-flight mass spectrometry. Rapid Commun. Mass Spectrom. *22*, 1553–1562. https://doi.org/10.1002/rcm.3523.
34. Lu, X., Liu, J., Ren, W., Yang, Q., Chai, Z., Chen, R., Wang, L., Zhao, J., Lang, Z., Wang, H., et al. (2018). Gene-Indexed Mutations in Maize. Mol. Plant *11*, 496–504. https://doi.org/10.1016/j.molp.2017.11.013.
35. Lahner, B., Gong, J., Mahmoudian, M., Smith, E.L., Abid, K.B., Rogers, E.E., Guerinot, M.L., Harper, J.F., Ward, J.M., McIntyre, L., et al. (2003). Genomic scale profiling of nutrient and trace elements in Arabidopsis thaliana. Nat. Biotechnol. *21*, 1215–1221. https://doi.org/10.1038/nbt865.
36. Bana, R.S., Jat, G.S., Grover, M., Bamboriya, S.D., Singh, D., Bansal, R., Choudhary, A.K., Kumar, V., Laing, A.M., Godara, S., et al. (2022). Foliar nutrient supplementation with micronutrient-embedded fertilizer increases biofortification, soil biological activity and productivity of eggplant. Sci. Rep. *12*, 5146. https://doi.org/10.1038/s41598-022-09247-0.
37. Bradbury, P.J., Zhang, Z., Kroon, D.E., Casstevens, T.M., Ramdoss, Y., and Buckler, E.S. (2007). TASSEL: software for association mapping of complex traits in diverse samples. Bioinformatics *23*, 2633–2635. https://doi.org/10.1093/bioinformatics/btm308.
38. Jin, M., Yan, S., Wu, Y., Zhai, Z., Alseekh, S., Chen, Y., Huang, W., Ma, N., Tao, K., Xiao, K., et al. (2026). Multiomics analysis of primary metabolism reveals the genetic basis of nitrogen partitioning modulated by ZmAVT1A-1 in maize. Nat. Genet. *58*, 1722–1733. https://doi.org/10.1038/s41588-026-02655-2.
39. Shin, J.-H., Blay, S., Graham, J., and McNeney, B. (2006). LDheatmap: An R Function for Graphical Display of Pairwise Linkage Disequilibria Between Single Nucleotide Polymorphisms. J. Stat. Soft. *16*, 1–9. https://doi.org/10.18637/jss.v016.c03.
40. Dobin, A., Davis, C.A., Schlesinger, F., Drenkow, J., Zaleski, C., Jha, S., Batut, P., Chaisson, M., and Gingeras, T.R. (2013). STAR: ultrafast universal RNA-seq aligner. Bioinformatics *29*, 15–21. https://doi.org/10.1093/bioinformatics/bts635.
41. Anders, S., Pyl, P.T., and Huber, W. (2015). HTSeq–a Python framework to work with high-throughput sequencing data. Bioinformatics *31*, 166–169. https://doi.org/10.1093/bioinformatics/btu638.
42. Love, M.I., Huber, W., and Anders, S. (2014). Moderated estimation of fold change and dispersion for RNA-seq data with DESeq2. Genome Biol. *15*, 550. https://doi.org/10.1186/s13059-014-0550-8.
43. Zhang, Q., Zhao, F., Wu, Z., and Zhu, D. (2022). A simple and robust method for isolating and analyzing chromatin-bound RNAs in Arabidopsis. Plant Methods *18*, 135. https://doi.org/10.1186/s13007-022-00967-y.
44. Liu, H., Ding, Y., Zhou, Y., Jin, W., Xie, K., and Chen, L.L. (2017). CRISPR-P 2.0: An Improved CRISPR-Cas9 Tool for Genome Editing in Plants. Mol. Plant *10*, 530–532. https://doi.org/10.1016/j.molp.2017.01.003.
45. Li, C., Liu, C., Qi, X., Wu, Y., Fei, X., Mao, L., Cheng, B., Li, X., and Xie, C. (2017). RNA-guided Cas9 as an in vivo desired-target mutator in maize. Plant Biotechnol. J. *15*, 1566–1576. https://doi.org/10.1111/pbi.12739.
46. Liu, H.J., Jian, L., Xu, J., Zhang, Q., Zhang, M., Jin, M., Peng, Y., Yan, J., Han, B., Liu, J., et al. (2020). High-Throughput CRISPR/Cas9 Mutagenesis

Please cite this article in press as: Chao et al., Nicotianamine-driven nickel transport to sink organs underpins maize productivity, Cell (2027), https://doi.org/10.1016/j.cell.2026.10.035

Streamlines Trait Gene Identification in Maize. Plant Cell *32*, 1397–1413. https://doi.org/10.1105/tpc.19.00934.

47. Clough, S.J., and Bent, A.F. (1998). Floral dip: a simplified method for Agrobacterium-mediated transformation of Arabidopsis thaliana. Plant J. *16*, 735–743. https://doi.org/10.1046/j.1365-313x.1998.00343.x.
48. Chao, Z.F., Chen, Y.Y., Ji, C., Wang, Y.L., Huang, X., Zhang, C.Y., Yang, J., Song, T., Wu, J.C., Guo, L.X., et al. (2023). A genome-wide association study identifies a transporter for zinc uploading to maize kernels. EMBO Rep. *24*, e55542. https://doi.org/10.15252/embr.202255542.
49. Cailliatte, R., Schikora, A., Briat, J.F., Mari, S., and Curie, C. (2010). High-affinity manganese uptake by the metal transporter NRAMP1 is essential for Arabidopsis growth in low manganese conditions. Plant Cell *22*, 904–917. https://doi.org/10.1105/tpc.109.073023.
50. Huang, Y., Wang, H., Zhu, Y., Huang, X., Li, S., Wu, X., Zhao, Y., Bao, Z., Qin, L., Jin, Y., et al. (2022). THP9 enhances seed protein content and nitrogen-use efficiency in maize. Nature *612*, 292–300. https://doi.org/10.1038/s41586-022-05441-2.
51. Deng, Y., Wang, J., Zhang, Z., and Wu, Y. (2020). Transactivation of Sus1 and Sus2 by Opaque2 is an essential supplement to sucrose synthase-mediated endosperm filling in maize. Plant Biotechnol. J. *18*, 1897–1907. https://doi.org/10.1111/pbi.13349.
52. Hogan, M.E., Swift, I.E., and Done, J. (1983). Urease assay and ammonia release from leaf tissues. Phytochemistry *22*, 663–667. https://doi.org/10.1016/S0031-9422(00)86958-7.
53. Lavres, J., Castro Franco, G., and de Sousa Câmara, G.M. (2016). Soybean Seed Treatment with Nickel Improves Biological Nitrogen Fixation and Urease Activity. Front. Environ. Sci. *4*. https://doi.org/10.3389/fenvs.2016.00037.
54. Salem, M.A., Jüppner, J., Bajdzienko, K., and Giavalisco, P. (2016). Protocol: a fast, comprehensive and reproducible one-step extraction method for the rapid preparation of polar and semi-polar metabolites, lipids, proteins, starch and cell wall polymers from a single sample. Plant Methods *12*, 45. https://doi.org/10.1186/s13007-016-0146-2.
55. Yan, S., Huang, W., Gao, J., Fu, H., and Liu, J. (2018). Comparative metabolomic analysis of seed metabolites associated with seed storability in rice (Oryza sativa L.) during natural aging. Plant Physiol. Biochem. *127*, 590–598. https://doi.org/10.1016/j.plaphy.2018.04.020.

Please cite this article in press as: Chao et al., Nicotianamine-driven nickel transport to sink organs underpins maize productivity, Cell (2027), https://doi.org/10.1016/j.cell.2026.10.035

STAR★METHODS

KEY RESOURCES TABLE

REAGENT or RESOURCE	SOURCE	IDENTIFIER
Antibodies		
Anti-NA antibody	This paper	Chao et al.[20]
Alexa Fluor 405-conjugated goat anti-mouse IgG secondary antibody	Abmart	Cat#M213411; RRID: AB_175660
Bacterial and virus strains		
Escherichia coli DH5α	Widely distributed	N/A
Escherichia coli DB3.1	Widely distributed	N/A
Agrobacterium tumefaciens EHA105	Widely distributed	N/A
Chemicals, peptides, and recombinant proteins		
KOD -Plus- Neo	TOYOBO	Cat#KOD-401
TRIZOL reagent	Invitrogen	Cat#15596018
DNase I digestion	Qiagen	Cat#79254
Phosphate-buffered saline (PBS)	TaKaRa	Cat#T900
Cellulose	Yakult	Cat#9012-54-8
β-glucuronidase	LabTop	Cat#S10046
Pectinase	LabTop	Cat#S10007
NBT solution	Roche	Cat#11383213001
Critical commercial assays		
Hieff Clone one-step PCR cloning kit	Yeasheng	Cat#10911ES25
RNeasy Mini Kit	Qiagen	Cat#74106
Quick RNA isolation Kit	Huayueyang	Cat#0416-50
Yeastmaker™ Yeast Transformation System 2	TaKaRa	Cat#630439
SYBR®Green Realtime PCR Master Mix	TOYOBO	Cat#QPK-201C
TransScript® One-Step gDNA Removal and cDNA Synthesis SuperMix	TransGen	Cat#AT311-02
Super Script III First Strand Kit	Invitrogen	Cat#18080-044
Total Starch Assay kit	Solarbio	Cat#BC0705
Experimental models: Organisms/strains		
Maize B73	This paper	N/A
Maize KN5585	This paper	N/A
Maize *zmnaet1-1*	This paper	https://maizeems.qlnu.edu.cn
Maize *zmnaet1-2*	This paper	https://maizeems.qlnu.edu.cn
Maize *crinaet1-1*	This paper	N/A
Maize *crinaet1-2*	This paper	N/A
Rice *osnaet1-1* and *osnaet1-2*	This paper	N/A
Rice *osnaet2-1* and *osnaet2-2*	This paper	N/A
Rice *osnaet1naet2-1* and *osnaet1naet2-2*	This paper	N/A
Maize pZmNAET1^{B73}::GUS	This paper	N/A
Maize *pUbi::ZmNAET1^{B73}-eYFP*	This paper	N/A
Maize *proAtNAET2::ZmNAET1^{B73}*	This paper	N/A
Maize Ji53	This paper	Liu et al.[19]
Maize Ji853	This paper	Liu et al.[19]
Maize HZS	This paper	Liu et al.[19]
Maize HYS	This paper	Liu et al.[19]

(*Continued on next page*)

Please cite this article in press as: Chao et al., Nicotianamine-driven nickel transport to sink organs underpins maize productivity, Cell (2027), https://doi.org/10.1016/j.cell.2026.10.035

Continued

REAGENT or RESOURCE	SOURCE	IDENTIFIER
Maize E28	This paper	Liu et al.[19]
Maize 81515	This paper	Liu et al.[19]
Maize 5237	This paper	Liu et al.[19]
Maize Zong3	This paper	Liu et al.[19]
Maize Zong31	This paper	Liu et al.[19]
Maize YFH	This paper	Liu et al.[19]
Maize Zi330	This paper	Liu et al.[19]
Maize Chang7-2	This paper	Liu et al.[19]
Maize HUANGC	This paper	Liu et al.[19]
Maize Xi502	This paper	Liu et al.[19]
Maize Q1261	This paper	Liu et al.[19]
Maize TYS	This paper	Liu et al.[19]
Maize NX110	This paper	Liu et al.[19]
Maize Lv28	This paper	Liu et al.[19]
Maize Lx9801	This paper	Liu et al.[19]
Maize F349	This paper	Liu et al.[19]
Maize Dan340	This paper	Liu et al.[19]
Maize H21	This paper	Liu et al.[19]
Maize Shuang741	This paper	Liu et al.[19]
Maize K12	This paper	Liu et al.[19]
Maize MG_1054	This paper	Liu et al.[19]
Maize MG_1212	This paper	Liu et al.[19]
Oligonucleotides		
Primers used in this study	See Table S17	N/A
Recombinant DNA		
pUbi::ZmNAET1^{B73}-eYFP	This paper	N/A
pZmNAET1^{B73}::GUS	This paper	N/A
pCPB-ZmUbi::hSpCas9-ZmNAET1	This paper	N/A
pCPB-ZmUbi::hSpCas9-OsNAET1	This paper	N/A
pCPB-ZmUbi::hSpCas9-OsNAET2	This paper	N/A
35s::AtNAET2-mCherry	This paper	N/A
proAtNAET2::ZmNAET1^{B73}	This paper	N/A
35s::ZmNAET1-GFP	This paper	N/A
pPR3-AhNAS3	This paper	N/A
pBT3-AtNAET2	This paper	N/A
pBT3-ZmNAET1	This paper	N/A
Software and algorithms		
GraphPad Prism 10	GraphPad Software	N/A
RStudio	RStudio	N/A
TASSEL 5.0	TASSEL	N/A

EXPERIMENTAL MODEL AND STUDY PARTICIPANT DETAILS

Plant materials and growth conditions

The complete-diallel design plus Unbalanced Breeding-like Inter-Cross (CUBIC) population[19] derived from extensive inter-crossing of 24 elite Chinese maize inbred lines was planted in nursery fields in Hainan (2014 and 2016, winter). All maize plants were planted in one-row plots (2.5 m per row with 0.25 m spacing between plants and 0.75 m between rows) at each location. Field management followed standard agronomic procedures. Daily environmental factor data for CUBIC populations were collected from planting to

Please cite this article in press as: Chao et al., Nicotianamine-driven nickel transport to sink organs underpins maize productivity, Cell (2027), https://doi.org/10.1016/j.cell.2026.10.035

harvest. As detailed in Table S15, five types of environmental factors were recorded: temperature, water, light, air, and soil. In addition, soil pH and the soluble elemental composition of the field soil are provided in Table S16.

Seeds of *zmnaet1-1* (EMS3-10a3b7) and *zmnaet1-2* (EMS3-08971a) were ordered from MEMD[34] (https://maizeems.qlnu.edu.cn). The homozygous EMS mutants and the wild accession B73 were planted in Shanghai, China, in 2020, 2021. Primers used for genotyping are listed in Table S17.

For the hydroponic experiment, KN5585 and *crinaet1-1* mutant were first germinated on filter paper for 3 days and then cultivated in modified Hoagland solution for 10 days. Ten plants were cultivated in each 5 L black bucket. The nutrient solution contained 1 mM $Ca(NO_3)_2 \cdot 4H_2O$, 3 mM $CaCl_2$, 5 mM KNO_3, 0.5 mM $MgSO_4 \cdot 7H_2O$, 0.25 mM $NH_4H_2PO_4$, 0.25 mM $NH_4H_2PO_4$, 10 μM Fe-HBED, 1.25 μM H_3BO_3, 1 μM $MnCl_2 \cdot 4H_2O$, 1 μM $ZnSO_4 \cdot 7H_2O$, 0.25 μM $CuSO_4 \cdot 5H_2O$, 0.1 μM $CoCl_2 \cdot 6H_2O$, 0.4 μM $(NH_4)_6Mo_7O_{24} \cdot 4H_2O$. The pH was adjusted to 5.8 using MES and KOH. The nutrient solution was replaced every 3 days. Whole-plant fresh weight and shoot height were measured.

The *Arabidopsis* plants used for elemental analysis were grown in a climate-controlled room under previously described growth conditions.[35] The plants were bottom-watered twice a week with modified 0.25 × Hoagland's Type 2 and 10 μM Fe-HBED. To prepare 1 L of working solution, 0.165 g $Ca(NO_3)_2 \cdot 4H_2O$, 0.029 g $NH_4H_2PO_4$, 0.152 g KNO_3, 0.123 g $MgSO_4 \cdot 7H_2O$ were added, together with 1 mL $CuSO_4 \cdot 5H_2O$ (0.75 g L^{-1} stock solution), 1 mL $ZnSO_4 \cdot 7H_2O$ (2.3 g/L stock solution), 1 mL H_3BO_3 (28.44 g L^{-1} stock solution), 1 mL $MnCl_2 \cdot 4H_2O$ (10.1 g L^{-1} stock solution), 1.25 mL MoO_3 (0.16 g L^{-1} stock solution) and 10 μM Fe-HBED.

Large-scale field trials for chemical complementation tests were performed in Bozhou, Anhui province (2025, summer) for preliminary testing and Kunming, Yunnan (2025, winter) for data collection. Three different spray treatments were tested: control application (with 18.2 MΩ Milli-Q water); Ni (0.003%), 5 μM $NiSO_4$; and Zn (0.3%), 460 μM $ZnSO_4$. The Zn concentration was used according to the methods described[36] with twice. Given Zn concentrations in plant tissues are approximately 100 times higher than Ni concentrations, a lower Ni concentration was used. The spraying test was performed in the morning using a hand-held sprayer. Stock solutions were prepared based on the elemental concentrations, and the appropriate volume of each stock solution was diluted to a final working volume of 200 mL for application to each plant. Spraying was performed weekly, beginning 1 week after germination and continuing until harvest. Each treatment consisted of 50 plants, with approximately 0.6 m × 0.25 m spacing between plants. Plant height was measured at the flowering stage. Urease activity and the contents of urea and amino acids were measured in shoot apex collected 4 weeks after germination; nodes collected at the flowering stage and ears collected 13 days after pollination. Elemental concentrations in the tassel and ears were measured.

For all maize seed germination assays, seeds were first imbibed in 50 mL of 18.2 MΩ Milli-Q water, with or without Ni or Zn supply for 12 h of imbibition. Then the seeds were transferred to plastic petri dishes with lids and incubated for the indicated periods.

METHOD DETAILS

Elemental profiling

For seed element detection, ten dry, mature kernels from each maize line were pooled and ground using a customized grinder equipped with a grinding tank made of polytetrafluoroethylene and Jargonia beads (Jingxin Industry Co., Ltd., Shanghai). For other tissues, fresh tissues from each plant were harvested as independent samples at the indicated developmental stage. Samples were fully dried and 2–5 mg of each sample was used for ICP–MS (inductively coupled plasma—mass spectrometry) analysis. At 8 weeks after germination, before flowering, tassels and bract leaves were collected. At the same stage, nodes that generated the shank or were located near the ears were collected. Stems, defined as the node together with the two adjacent internodes, were also sampled for ionomic analysis. Ears were harvested 13 days after germination for elemental analysis. All samples were first dried at 65 °C to constant weight and then powdered using the customized grinder described above.

The rinsed or powdered samples were transferred to Pyrex test tubes (16× 100 mm) and dried in an oven at 65°C for 24 h. Twelve samples were weighed, and their weights were used to estimate the weights of the remaining samples. Trace metal grade nitric acid Primar Plus (Fisher Chemicals) spiked with indium internal standard was added to each tube (1 mL per tube). Samples were digested in a block heater (DigiPREP MS, SCP Science; QMX Laboratories, Essex, UK) at 115°C for 5 h. The digested samples were diluted to a final volume of 10 mL with 18.2 MΩ Milli-Q Direct water (Merck Millipore). Elemental analysis was performed using ICP–MS (NexION 350D; PerkinElmer, USA) equipped with an Apex desolvation system and an SC-4 DX autosampler (Elemental Scientific Inc., USA). All solid samples were normalized using a heuristic algorithm based on the best-measured elements, as previously described.[7] For each set of ICP–MS measurements, the median value from each run was used to correct for run-to-run variations. The corrected values were then $\log_2$-transformed, and extreme outliers were removed via the usage "rosnerTest" of the EnvStats package (Millard, 2014) in R. Finally, all the clean data were processed for subsequent analysis.

Genome-wide association study

The $\log_2$-transformed values of kernel Ni in CUBIC population (Kernel_1 and Kernel_2) were used for genome-wide association studies (GWAS). The original concentration data are listed in Table S1. Approximately 10.8 million high-quality SNPs (MAF≥0.05), and the same relatedness matrix and the top ten principal components used in the previous study[19] were routinely fitted into the mixed linear model (MLM) of the software TASSEL 5.0[ref].[37] The significance threshold for the association was set to 1/N (P = 9.3e-08), where N represents the number of genome-wide SNPs used in the MLM.

Please cite this article in press as: Chao et al., Nicotianamine-driven nickel transport to sink organs underpins maize productivity, Cell (2027), https://doi.org/10.1016/j.cell.2026.10.035

LD analysis and QTL definition

To clearly interpret the numerous significant associations, significant SNPs were first grouped within 20-kb sliding windows, and the windows containing at least two consecutive significant SNPs were retained. Adjacent significant windows were then merged when their LD satisfied $R^2 \geq 0.2$, resulting in a continuous LD block that was designated as a QTL. This approach is consistent with the QTL definition used in our previous studies.[19,38] Pairwise LD analysis data are listed in Table S3. Eight significant SNPs variants were selected based on their strong associations with kernel Ni content in the CUBIC population in 2016. Among these, five SNPs (−1086, −1073, −1035, −1025, and −108) were in the promoter region of ZmNAET1 and three SNPs (379, 1516, and 1696) were located within the gene body. Pairwise linkage disequilibrium (LD) among these eight SNPs was calculated as r^2 and visualized using the 'LDheatmap ()' function[39] in R.

RNA-Seq and RT-qPCR analysis

Tissue samples of young and old leaves, roots, ears, endosperm, embryos, stems from 24 parental inbred lines of the CUBIC population were collected for total RNA extraction and RNA-seq analysis. RNA extraction was performed according to the standard protocol of the Quick RNA Isolation Kit, #0416-50 (Huayueyang Biotechnology Co., LTD. Beijing, China). A library with insert sizes from 200 to 500 bp was generated using Illumina library preparation kits (TruSeq Stranded mRNA LT-SetA. RS-122-1201). The 150 bp paired-end sequence reads were mapped onto the B73 AGPv3.25 reference using STAR.[40] Gene expression levels were quantified using HTSeq protocol,[41] expression data for each gene were normalized using DESeq2.[42]

The roots, shoots, leaves, nodes, stalks, shanks, silks and tassels from B73 plants were collected and flash-frozen in liquid nitrogen. Roots and shoots were collected at the 2 weeks seedlings. Shoot apex and basal nodes were collected from 4-week-old plants. Silks and tassels were collected at the flowering and pollination stage. The bract leaves, stems and stalks near the ears, shanks were collected at different days after pollination. Total RNA was extracted using TRIzol reagent (Invitrogen: 15,596,018) and purified using the RNeasy Mini Kit (Qiagen: 74,106) after DNAse I digestion (Qiagen: 79,254). For RT-qPCR analysis of *ZmNAET1* expression, extracted RNA was reverse-transcribed using the Super Script III First Strand Kit (Invitrogen). The resulting cDNA was diluted to 50 ng μL^{-1} for RT-qPCR with SYBR Green (TOYOBO) on a CFX Connect Real-Time System (Bio-Rad). The maize gene *ZmSGT1* (*Zm00001d044172*) was used as the internal control. Relative gene expression levels were calculated using the $2^{-\Delta Ct}$ method. All experiments were performed using three independent RNA samples. Primers are listed in Table S17.

Detection of pre-mRNA was strictly performed following the method described.[43] Briefly, the extraction of chromatin bound RNAs mainly involves a step for nuclear extraction, followed by two stringent wash steps. Stems of maize plants were first collected and flash-frozen in liquid nitrogen. After being finely ground into powder, 2 g of the tissue were transferred to a 50 mL tube containing 10 mL of Honda buffer. The mixture was then vortexed and filtered through Miracloth, followed by centrifugation at 3500 g for 5 min at 4°C. The resulting pellet was resuspended in 20 mL of Honda buffer and centrifuged again. The pellet was resuspended with 1 mL of Honda buffer and centrifuged at 8000 g for 1 min at 4°C. After weighing the pellet, one volume of nuclei resuspension buffer and two volumes of washing buffer were added, followed by centrifugation. The pellet was then resuspended in one volume of resuspension buffer and centrifuged again. The resulting chromatin fraction was used for nuclear RNA extraction according to the standard RNA extraction protocol. The primers used are listed in Table S17.

The methods for detecting allelic mRNA and pre-mRNA abundance in F1 progenies of MG_1054 and MG_1212 are like that for regular RT-qPCR, with allele-specific primer pairs designed for the two haplotypes. In brief, when designing primers, the antisense primer is designed to be identical for both alleles, while the 3′-terminal nucleotide of the sense primer was positioned directly over the haplotype-specific SNP. This design thereby generates two pairs of amplification primers that can specifically amplify the transcript of Hap1 and the transcript of Hap2, respectively. The specificity of the primers was tested using RNA from the two parental lines. The primers used are listed in Table S17.

Vector construction and plant transformation

For gene editing in maize, the targets of *ZmNAET1, OsNPF5.8/9* for the sgRNA construct were designed via CRISPR 2.0[44] and introduced into two sgRNA expression cassettes by overlapping PCR. The two sgRNA expression cassettes were then integrated into the *pCPB-ZmUbi::hSpCas9* vector.[45] In addition, to construct the overexpression vectors of *ZmNAET1*, the full-length gene of *ZmNAET1* was amplified from B73 and inserted into the *proZmUbi::eYFP* vector to generate the *pUbi::ZmNAET1-eYFP* constructs. To construct the *pZmNAET1*::GUS vector, a 2-kb promoter of *ZmNAET1* was amplified from B73 and inserted into the pCAMBIA1303*::GUS* vector to generate the *pZmNAET1*::GUS constructs. The primers used are listed in Table S17. The three constructs were separately transferred to the *Agrobacterium* strain EHA105 and transformed into the immature embryo of the maize inbred line KN5585[46] through Agrobacterium-mediated transformation by WIMI Biotechnology Co., Ltd. The knockout mutants and overexpression lines of the T_3 generation were planted under isolation conditions in Shanghai, China, in 2021 and 2022.

To construct the *proAtNAET2::ZmNAET1* constructs, a 2-kb promoter of *AtNAET2* was amplified from Col-0 genomic DNA and inserted into the pCAMBIA1300 empty vector to generate the *proAtNAET2::ZmNAET1* construct. The construct was first transformed into the *Agrobacterium tumefaciens* strain GV3101 and then introduced into *naet1naet2* plants using the floral dip method.[47]

To construct the *AtNAET2-mCherry* vector, the coding sequence of AtNAET2 was amplified from Col-0 cDNA and inserted into the *pCAMBIA1300-35s::mCherry* empty vector to generate the *35s::AtNAET2-mCherry* construct. To construct the *ZmNAET1-GFP* vector, the coding sequence of *ZmNAET1* was amplified from B73 cDNA and inserted into the *pCAMBIA1300-35s::GFP*

Please cite this article in press as: Chao et al., Nicotianamine-driven nickel transport to sink organs underpins maize productivity, Cell (2027), https://doi.org/10.1016/j.cell.2026.10.035

empty vector to generate the *35s::ZmNAET1-GFP* construct. For transient expression of genes in *N. benthamiana* leaf epidermal cells, the expression vectors were first transformed into GV3101 and then leaves of 4-week-old plants were infiltrated with corresponding strains. At 36 h after injection, the signal was observed under a confocal laser scanning microscope (Leica TCS SP8). Primers are listed in Table S17.

Yeast expression and NA detection

The yeast expression vectors *pPR3-AhNAS3 and pBT3-AtNAET2* were constructed as previously described. For construction of *pBT3-ZmNAET1*, the coding region was amplified from B73 cDNA and inserted into the yeast expression vector *pBT3-STE*. *pBT3-ZmNAET1*, *pBT3-AtNAET2* and *pBT3-STE* were separately introduced into yeast strain NMY51 with *pPR3-AhNAS3*, and the transformants were cultured in YPD liquid medium. Primers are listed in Table S17.

Detection of NA was performed following the method described previously.[20] The liquid medium culturing yeast strains with different constructs was first concentrated for 15 min at 3500 g and OD = 0.8. Then the supernatant of the yeast culture was further concentrated for 20 min at 13,400 g and 4°C. For the concentrated yeast cells, after freeze-drying for 4 h, ~100 mg of fresh sample was ground in liquid nitrogen and extracted with 300 μL of ultrapure water at 80°C with shaking for 30 min, followed by 20 min of concentration at 13,400 g at 4°C. The concentrated supernatant solution from the liquid medium and yeast cells were separately transferred to centrifuge tubes with filters (0.22 μm) and further centrifuged for 10 min at 13,400 g. The filtered supernatant solution was determined in an ultra-performance liquid chromatography—mass spectrometer (UPLC–MS; QTRAP 6500+, AB SCIEX) using a Thermo Hypercarb C18 column (150 mm*2.1 mm, 5 μm; Thermo Fisher, USA) with an amino acid analysis kit. The solvents were water (A) and acetonitrile (B), both acidified with 0.1% (v/v) formic acid. Chemically synthesized NA (Cayman, USA) was used as a standard.

Immunostaining of NA

Immunostaining of NA was performed following the method described previously with modifications.[20,48] The custom affinity-purified polyclonal anti-NA antibodies were produced by Youke Biotechnology Co., Ltd. (Shanghai, China). In brief, one-week-old leaves of transgenic plants overexpressing ZmNAET1 were fixed for 1 h in freshly prepared 4% (v/v) formaldehyde in PHEM buffer (60 mM PIPES, 25 mM HEPES, 10 mM EGTA, 2 mM $MgCl_2$; pH 6.9) with 0.02% (v/v) Triton X-100 and 5% (v/v) DMSO. After being rinsed several times in PHEM buffer, the samples were digested in enzyme solution containing 1% (w/v) β-glucuronidase (LabTop, catalog number S10046), 0.1% (w/v) cellulose (Yakult, catalog number 9012-54-8), 0.1% (w/v) pectinase (LabTop, catalog number S10007), 0.1% (w/v) lyticase (Yeasen, catalog number 10403ES92), and 1% (w/v) glucose at 37°C for 30 min to remove cell walls, followed by washing with PHEM buffer. Samples were put into PHEM buffer with 1% Triton X-100, 5% DMSO and 3% BSA (w/v) at 37°C for 30 min. After washing again with PHEM buffer, the samples were placed in PBS (10 mM Na_2HPO_4, 1.8 mM KH_2PO_4, 2.7 mM KCl, 137 mM NaCl; pH 7.4) with anti-NA antibody (1:200) and incubated overnight in the dark at 4°C. Then, the samples were washed 5 times with PBS and incubated with Alexa Fluor 405-conjugated goat anti-mouse IgG secondary antibody (Abmart Co., Ltd., Shanghai) at a dilution of 1:300 in PBS for 1 h at 37°C. After washing 5 times in PBS, the samples were then observed using a confocal laser scanning microscope (TSC SP8 STED 3X, Leica). To observe the secondary antibody signals, an excitation wavelength of 405 nm from an argon laser was used, and the emission signal was detected at 420–460 nm.

Cell imaging

Cellular fluorescence was observed under a Leica TCS SP8 confocal laser scanning microscope. To observe the GFP signals, an excitation wavelength of 488 nm from an argon laser was used, and the emission signal was detected at 500–550 nm. mCherry was stimulated with an excitation wavelength of 561 nm, and its emission signal was detected at 570–620 nm. For immunostaining of NA, the secondary antibody labeled with Alexa Fluor™ 405 (Abmart Co., Ltd., Shanghai) was stimulated by a 405 nm argon laser and observed at 421–450 nm.

GUS histochemical staining was performed as previously described.[49] Pictures were taken for the tissues with GUS signals under a stereo microscope (SMZ1500, Nikon, Japan).

Phylogeny analysis

Protein sequences of ZmNAET1 homologs were retrieved from the public plant genome database Gramene (www.gramene.org). Phylogenetic relationships were analysed using the neighbor-joining method and was computed using the Poisson correction method. Phylogenetic analyses were then conducted using the Molecular Evolutionary Genetics Analysis X software (www.megasoftware.net).

Measurement of N, protein and starch

Total N content was detected in selected tissues at different developmental stages. Shoot apex was harvested 4 weeks after germination. The 3rd leaf, 12th leaf, node and tassel were collected at the flowering stage. The node sample was the one produces the shank. Ears was harvested at 13 days after pollination and the mature seeds were collected. Samples were first fully dried at 65 °C and then powdered using a customized grinder as introduced in elemental detection. Approximately 50–70 mg of powdered

sample was used for total nitrogen measurement using an ELEMENTAR Rapid N exceed instrument following standard method.[50] Total protein content in mature seeds was detected using the same method. The seeds' endosperm powder was filtered through an 80-mesh sieve and the starch content was measured with a Total Starch Assay kit (BC0705, Solarbio) following the standard protocol.[51]

Urea and amino acids detection

For the detection of urea and amino acids in maize kernels, 10 seeds from one ear were pooled as one biological sample. After imbibition and freeze-drying, the seeds were grinded into a fine powder using the customized grinder. Other tissues were processed using the same procedure, except the imbibition was omitted. Approximately 50 mg of fresh sample was extracted with 500 μL of ultrapure water at 4°C with shaking for 30 min, followed by 20 min of concentration at 14,000 g at 4°C. Then 380 μL of the supernatant was added with 720 μL acetonitrile and further concentrated for 20 min at 14,000 g and 4°C. A 100 μL aliquot of the concentrated supernatant solution was transferred to centrifuge tubes equipped with filters (0.22 μm) and further centrifuged for 10 min at 14,000 g. The filtered supernatant solution was analysed using ultra-performance liquid chromatography—mass spectrometer (UPLC–MS; QTRAP 6500+, AB SCIEX) using a Thermo Hypercarb C18 column (Thermo Fisher, USA) with an amino acid analysis kit. The solvents were water, 5% acetonitrile and 95% acetonitrile, all acidified with 0.1% (v/v) formic acid (FA) and 5 mM NH_4FA. The column was maintained at 40 °C with a flow rate of 0.3 mL min^{-1}, and the gradient of B was as follows: 0 min, 100%; 1.5 min, 100%; 17 min, 75%; 19 min, 40%; 20 min, 40%; 20 min, 100%; 25 min, 100%. All analytes were detected using Multiple reaction monitoring (MRM) mode. The optimized ESI operating parameters for positive mode were ion spray voltage, 5 kV; ion spray temperature, 500 °C; curtain gas, 35 psi; ion source gas 1, 50 psi; ion source gas 2, 50 psi. The compound identities were verified by mass, and retention time matches to authenticated standards. Instrument control and data acquisition were performed using Analyst 1.6.3 software (AB SCIEX), and data processing was performed using MultiQuant 3.0.2 software (AB SCIEX).

Detection of urease activity

Urease activity in vivo was measured according to the methods described.[52,53] The fresh seeds (10 seeds from one ear were pooled as one independent sample) and other fresh tissues were first cut into 1–2 mm slices using a ceramic knife. Approximately 200 mg of fresh tissue was placed in a tube containing 8 mL of NaH_2PO_4 buffer with 0.5 M urea, pH 7.4. The solution was incubated for 3 h at 30°C in the dark with constant agitation. After incubation, 0.5 mL of the extract was put into a tube containing the reaction buffer: 2.5 mL of Reagent I (phenol 0.1 mol L^{-1}, sodium nitroprusside 170 μmol L^{-1}) and 2.5 mL of Reagent II (NaOH 0.125 mol L^{-1}, $Na_2HPO_4 \cdot 12H_2O$ 0.15 mol L^{-1}, NaClO with 3% Cl_2). The tubes were immediately sealed to avoid loss of NH_3 and placed in a water bath at 37°C for 35 min. After that, the solution was measured at 625 nm by colorimetry in a spectrophotometer. Urease activity was determined by the amount of NH_4^+ produced using a standard curve generated with different concentrations of NH_4Cl. Urease activity was represented as μmol NH_4^+ g^{-1} FW h^{-1}.

GC-MS

The metabolites change during seed germination were detected by GC-MS. Germinating kernels (KN5585 and *crinaet1-1*) (stored one year) at 1 hr, 12 hrs, 24 hrs, 44 hrs and 60 hrs after imbibition were sampled and freeze-dried under liquid nitrogen before metabolic extraction. Samples were finely ground using a Mixer mill (MM400; Retsch) for 45 seconds at 30 Hz. Approximately 50 mg of each powdered sample was extracted following the procedures described in previous studies.[54] Briefly, samples were added into 1 mL of extraction solvent mixture 1 (methyl tert-butyl ether were added to methanol, 3:1, vol/vol) and thoroughly vortexed for 1 min. Then, incubate on an orbital shaker (100 rpm, 45 min) at 4 °C followed by a 15 min sonication step. For phase separation, a volume of 650 μl of solvent mixture 2 (water were added to methanol, 3:1, vol/vol)) was added to each vial/tube and the samples were again thoroughly vortexed for 1 min. After that, the samples are centrifuged at a speed of 20,000*g* for 5 min at 4 °C. For primary metabolite profiling, dried pellets were derivatized with N-methyl-N-(trimethylsilyl) trifluoroacetamide as described previously,[55] and further analysed using GC-MS (7890A-5975C, Agilent, USA). Briefly, the dried pellets were re-suspended in methoxyamine-hydrochloride/pyridine solution for methoxymization of carbonyl groups followed by heating at 37 °C for 90 min. The samples were further derivatized with N-methyl-N-(trimethylsilyl) trifluoroacetamide for 30 min at 37 °C. A 1 μL aliquot of each sample was injected into GC-MS at 270°C in split mode (50: 1) with helium carrier gas (> 99.999% purity) flow set to 1 mL min^{-1} and separated by a DB-35MS UI (30 m × 0.25 mm, 0.25 μm) capillary column. The Agilent MassHunter Quantitative Analysis software (version B.07.01) was used for GC-MS data analysis. NIST library and an in-house database established using authentic standards were used together for metabolite identification.

QUANTIFICATION AND STATISTICAL ANALYSIS

Data for quantification analyses are represented as mean ± SD. Statistical significance was assessed using Student's *t*-test for comparisons between two groups, with *P* values indicated in the figures. Statistical significances were determined by one-way ANOVA followed by Tukey's post hoc test. Statistical significance was assessed by two-way ANOVA followed by Tukey's multiple comparisons test. Different letters at top of columns indicate significant differences at $P < 0.05$. The statistical analyses for all experiments were performed with the GraphPad Prism 10 software. The exact value of *n*, what *n* represents, and the statistical details of each experiment are described in the figure legends or methods.